Avoidance of hydrogen sulfide is modulated by external and internal states in *C. elegans*

Longjun Pu[1, 2, 3], Lina Zhao[1, 2, 3], Jing Wang[1, 2, 3], Clementine Deleuze[6], Lars Nilsson[1, 2, 3], Johan Henriksson[1, 4, 5], Patrick Laurent[6*], Changchun Chen[1, 2, 3*]

[1]Department of Molecular Biology, Umeå University, Umeå, Sweden

[2]Umeå Centre for Molecular Medicine, Umeå University, Umeå, Sweden

[3]Wallenberg Centre for Molecular Medicine, Umeå University, Umeå, Sweden

[4]The Laboratory for Molecular Infection Medicine Sweden (MIMS), Umeå University, Umeå, Sweden

[5]Integrated Science Lab (Icelab), Umeå University, Umeå, Sweden

[6]Laboratory of Neurophysiology, ULB Neuroscience Institute (UNI), Université Libre de Bruxelles (ULB), Belgium

*Corresponding author

E-mail: patrick.laurent.ulb@gmail.com; Changchun.chen@umu.se

Abstract

Hydrogen sulfide (H_2S) acts as an energy source, a toxin, and a gasotransmitter across diverse biological contexts. We use the robust locomotory responses of *Caenorhabditis elegans* to high levels of H_2S to elucidate the molecular mechanisms underlying its acute perception and adaptive responses. We find that the H_2S-evoked behavioral response is shaped by multiple environmental factors including oxygen (O_2) levels and nutritional state, and is modulated by various pathways such as insulin, TGF-β, and HIF-1 signaling, as well as by input from O_2-sensing neurons. Prolonged exposure to H_2S activates HIF-1 signaling, leading to the upregulation of stress-responsive genes, including those involved in H_2S detoxification. This promotes an adaptive state in which locomotory speed is reduced in H_2S, while responsiveness to other stimuli is preserved. In mutants deficient in HIF-1 signaling, iron storage, and detoxification mechanisms, animals display a robust initial response but rapidly enter a sleep-like behavior characterized by reduced mobility and diminished responsiveness to subsequent sensory stimuli. Furthermore, while acute production of mitochondria-derived reactive O_2 species (ROS) appears to initiate the avoidance response to H_2S, persistently high ROS promotes an adaptive state, likely by activating various stress-response pathways, without substantially compromising cellular H_2S detoxification capacity. Taken together, our study provides comprehensive molecular insights into the mechanisms through which *C. elegans* detects, modulates, and adapts its response to H_2S exposure.

Introduction

During the late Proterozoic era, the rise in oxygen (O_2) levels eliminated hydrogen sulfide (H_2S) from most habitats. Yet, low O_2 levels, along with high concentrations of hydrogen sulfide (H_2S) and carbon dioxide (CO_2), can persist in enclosed environments where bacteria actively decompose organic matter (Olson & Straub, 2016). H_2S can easily permeate biological membranes and interfere with various cellular processes. One of the most detrimental effects of H_2S is the disruption of cellular respiration by remodeling the mitochondrial electron transport chain and inhibiting cytochrome *c* oxidase (COX) (Cooper & Brown, 2008; Khan et al., 1990; Nicholls & Kim, 1982; Romanelli-Cedrez, Vairoletti, & Salinas, 2024).

The detection and response to chemical signals are crucial for various organisms to interact effectively with their environment. Animals living in H_2S-rich environments have evolved mechanisms to either avoid or adapt to these conditions, conferring them survival advantages. Species that encounter periodic increases in H_2S often possess sensing abilities and exhibit avoidance behaviors. For example, benthic species undertake daily vertical migrations between sulfidic and non-sulfidic waters (Abel, Koenig, & Davis, 1987; Salvanes, Utne-Palm, Currie, & Braithwaite, 2011). Certain metazoan species have seized the ecological opportunities presented by H_2S-rich environments through the development of cellular adaptations. Livebearing fish species, for instance, have evolved COX subunits that are more resistant to H_2S and more efficient at H_2S detoxification (Kelley et al., 2016; Pfenninger et al., 2014).

Free-living nematodes feed on bacteria that thrive in decaying organic matter, such as compost. This complex and dynamic environment, where species like *C. elegans* are commonly found, may exhibit significant fluctuations in H_2S levels over short distances (Adams, Farwell, Pack, & Bamesberger, 1979; Budde & Roth, 2011; Morra & Dick, 1991; Patange, Breen, Arsuffi, & Ruvkun, 2025; Rodriguez-Kabana, Jordan, & Hollis, 1965; Romanelli-Cedrez et al., 2024). Evidence suggests that *C. elegans* has evolved tolerance to prolonged H_2S exposure by reprogramming gene expression through H_2S-induced stabilization of the hypoxia-inducible factor HIF-1 (Budde & Roth, 2010; Powell-Coffman, 2010), and by developing an H_2S-

resistant electron transport chain (Romanelli-Cedrez et al., 2024). In particular, low concentrations of H_2S are not only well tolerated but can also be beneficial. For instance, exposure to 50 ppm H_2S has been shown to extend the lifespan and enhance thermotolerance (Budde & Roth, 2010; Fawcett, Hoyt, Johnson, & Miller, 2015; Horsman, Heinis, & Miller, 2019; Miller & Roth, 2007; Qabazard et al., 2014). Moreover, endogenous H_2S production in *C. elegans* modulates its interactions with actinobacteria (Patange et al., 2025). However, exposure to concentrations exceeding 150 ppm proved lethal (Budde & Roth, 2010, 2011; Fawcett et al., 2015; Horsman et al., 2019; Miller, Budde, & Roth, 2011a; Miller & Roth, 2007).

In addition to long-term adaptive mechanisms, *C. elegans* exhibits an acute behavioral response to H_2S exposure (Budde & Roth, 2011). In this study, we investigated whether and how the nematode *C. elegans* acutely avoids environments rich in H_2S, how it adapts at the molecular and physiological levels to H_2S exposure, and how these adaptations alter the avoidance response.

Results

C. elegans increases locomotory activity in response to acute H_2S exposure

In response to aversive cues, *C. elegans* initiates a pirouette followed by an increase of its locomotory speed to escape the noxious stimuli. When acutely exposed to 150 ppm H_2S, the laboratory N2 strain exhibited an increased locomotory speed and enhanced turning behavior, while generally decreasing the frequency of reversals, as a strategy to escape the noxious stimuli (***Figure 1A–C, Figure 1—Video 1***). The maximum speed was reached after 6–8 minutes in H_2S and returned to the baseline over a period of approximately 1 hour (***Figure 1D***). The reduced locomotory speed after 30 minutes in 150 ppm H_2S was reversible when these animals were immediately challenged with another stimulus, such as near-UV light (***Figure 1E***), suggesting that neuromuscular function remains preserved. The magnitude and dynamics of the H_2S-induced avoidance responses were concentration-dependent. Under our assay conditions, 50 ppm H_2S did not elicit an acute speed increase, and responses to 75 ppm were variable. In contrast, exposure to 150 ppm H_2S consistently triggered a robust and reproducible

93 escape response (***Figure 1F***), consistent with earlier reports that H_2S at 50 ppm exerts
94 beneficial effects, while H_2S at 150 ppm is toxic to *C. elegans* (Budde & Roth, 2010; Fawcett
95 et al., 2015; Horsman et al., 2019; Miller & Roth, 2007; Qabazard et al., 2014). To investigate
96 whether low levels of H_2S might be preferable or even attractive to the animals, we exposed
97 wild type animals to a linear gradient of H_2S (***Figure 1G***; See methods for details) (Bretscher,
98 Busch, & de Bono, 2008; Chang, Chronis, Karow, Marletta, & Bargmann, 2006; Gray et al.,
99 2004). Animals were allowed to move freely on a thin layer of bacteria within a microfluidic
100 chamber containing an H_2S gradient ranging from 150 ppm at one end to 0 ppm at the other.
101 As expected, *C. elegans* robustly avoids 150 ppm H_2S but does not accumulate at the extreme
102 end of 0 ppm ***(Figure 1G, H).*** The highest proportion of animals was found in the region with
103 approximately 40 ppm H_2S. These data suggest that H_2S acts as a potent repellent for *C. elegans*
104 at high concentrations but as an attractant at low levels.
105
106 **Candidate gene screen identifies signaling pathways required for H_2S-evoked locomotion**
107 To investigate the molecular mechanisms underlying the H_2S-evoked locomotory response in
108 *C. elegans*, we conducted a candidate gene screen for mutants that failed to increase their
109 locomotory speed upon exposure to an acute rise of H_2S level to 150 ppm. Our analysis
110 prioritized genes that are either known to be, or potentially involved in, sensory responses to
111 gaseous stimuli in both *C. elegans* and mammals (***Supplementary file 1***). We began by
112 examining mutants affecting globins, guanylate cyclases, and cyclic nucleotide-gated (CNG)
113 channels, which are involved in O_2 or CO_2 sensing in *C. elegans*, as well as wild isolates and
114 other previously characterized mutants with defective responses to gas stimuli (***Supplementary***
115 ***file 1***) (Bretscher et al., 2008; Gray et al., 2004; Hallem & Sternberg, 2008; Persson et al., 2009).
116 Given the essential role of K^+ channels in acute hypoxia sensing in mammals, we also screened
117 all potassium (K^+) channel mutants (Gao, Gonzalez-Rodriguez, Ortega-Saenz, & Lopez-Barneo,
118 2017; Weir, Lopez-Barneo, Buckler, & Archer, 2005). To explore how the H_2S sensory signals
119 were transmitted within the neural circuit, we assayed mutants with defects in ciliogenesis or
120 cilia-mediated signaling, as well as animals deficient in neurotransmission involving classical

121 neurotransmitters, neuropeptides, or biogenic amines. Finally, considering that mitochondrial
122 function is central to H_2S detoxification, we included mitochondrial electron transport chain
123 (ETC) mutants and key factors implicated in H_2S and superoxide clearance. Together, these
124 functionally diverse categories allowed us to survey a wide spectrum of potential mechanisms
125 contributing to the behavioral response to H_2S.

126 In the screen, a collection of mutants displayed reduced speed response, whereas only
127 a few exhibited a lack of omega-turn and/or reversal responses to H_2S (***Supplementary file 1***).
128 The reversal inhibition upon H_2S exposure and its rebound following H_2S withdrawal appeared
129 to vary substantially across experiments for N2, suggesting that differences in population
130 density, food availability, and animals' physiological state prior to the assay may matter.
131 Nevertheless, our screen revealed that signaling pathways, including cGMP, insulin and TGF-
132 β signaling, contributed to H_2S-evoked avoidance (***Supplementary file 1***). A naturally
133 occurring variant of the neuropeptide receptor gene *npr-1*, previously implicated in the
134 modulation of O_2 and CO_2 sensing, also affected locomotory speed in H_2S (***Supplementary file***
135 ***1***). In addition, mitochondrial components, including those involved in respiration and H_2S
136 detoxification, played critical roles in triggering and maintaining escape behavior in H_2S. In
137 contrast, we did not find evidence that globins, K^+ channels, or biogenic amine signaling
138 contributed significantly to the behavioral avoidance to H_2S (***Supplementary file 1***).

139

140 **cGMP signaling in ASJ cilia contributes to H_2S avoidance**

141 One group of mutants exhibiting reduced locomotory speed in H_2S had defects in ciliogenesis
142 (***Figure 2A–C***). This group included *daf-19* mutants lacking cilia, *dyf-3* mutants with reduced
143 cilia length, and *dyf-7* mutants in which ciliogenesis occurs but the cilia are not anchored to
144 their sensilla and are not exposed to the external environment (Heiman & Shaham, 2009;
145 Murayama, Toh, Ohshima, & Koga, 2005; Starich et al., 1995; Swoboda, Adler, & Thomas,
146 2000). These findings suggest that ciliogenesis and exposure of cilia to the external
147 environment are essential for animals to escape H_2S exposure. In addition, these mutants
148 exhibited consistently high reversal rate, likely associated with their reduced locomotory speed

149 (***Figure 2—figure supplement 1A–F***). Cilia-mediated sensory responses often involve the
150 activation of guanylate cyclases and the opening of cGMP-gated channels (Ferkey, Sengupta,
151 & L'Etoile, 2021). We observed significantly attenuated locomotory speed in response to H_2S
152 in *tax-4* or *tax-2* mutants, which lack key subunits of cilia-enriched cGMP-gated channels
153 (***Figure 2D, E***). In a comprehensive survey of all guanylate cyclase mutants, the *daf-11* strain
154 emerged as the only mutant showing speed response defects in the avoidance of H_2S (***Figure***
155 ***2D, supplementary file 1***). Similar to the cilia mutants, animals deficient in *daf-11* had low
156 speed, attenuated omega turns, and constantly high reversal rate (***Figure 2D, Figure 2—figure***
157 ***supplement 1G, H***). Selective expression of *daf-11* in ASJ neurons, but not in other neurons,
158 partially restored the speed response to acute H_2S (***Figures 2F, Figure 2—figure supplement***
159 ***2A–D***). In addition, the H_2S response defect of *tax-4* mutants was also rescued by selective
160 expression of its cDNA in ASJ neurons (***Figure 2G***), suggesting that the receptor guanylate
161 cyclase DAF-11 and the CNG channel TAX-4 act at least partially in ASJ neurons to promote
162 acute avoidance to H_2S. To validate the role of ASJ neurons in H_2S responses, we blocked
163 neurotransmission from ASJ using the catalytic domain of *Tetanus Toxin (TeTx*), which impairs
164 neurosecretion by specifically cleaving synaptobrevin (Schiavo et al., 1992). Cell-specific
165 expression of *TeTx* in ASJ significantly inhibited the speed response to H_2S ***(Figure 2H)***.
166 Surprisingly, using the Ca^{2+} sensor GCaMP6s to monitor a direct response of ASJ neurons to
167 H_2S, we observed no H_2S-induced Ca^{2+} transients under any of the tested conditions, whereas
168 CO_2-evoked Ca^{2+} increases were readily detected ***(Figure 2—figure supplement 2E, F).*** These
169 findings suggest that although ASJ neuronal activity and neurosecretion contribute to the H_2S
170 responses, ASJ neurons are unlikely to serve as the primary H_2S sensor.
171

172 **Starvation modulates H_2S avoidance**

173 In the candidate gene screen, another set of mutants with reduced speed responses to H_2S had
174 previously been shown to be defective in response to CO_2 (Hallem & Sternberg, 2008).
175 Specifically, the H_2S-evoked speed response was reduced in mutants deficient in nutrient-
176 sensitive signaling, including the insulin receptor DAF-2, the TGF-β ligand DAF-7, and the

177 nuclear hormone receptor NHR-49 (***Figure 3A–C, Figure 3—figure supplement 1A***).
178 Similarly, mutants lacking other CO_2 response modulators, such as the calcineurin subunits
179 TAX-6 and CNB-1, also failed to respond to H_2S (***Figure 3—figure supplement 1B, C***). In
180 addition to the abolished speed response, we also observed that the H_2S-evoked omega-turn
181 response was nearly abolished in *daf-2* mutants, and high proportion of animals exhibited
182 persistently high reversal rate regardless of H_2S stimulation (***Figure 3—figure supplement 1D–***
183 ***F***). The H_2S avoidance defects observed in *daf-2* and *daf-7* single mutants were fully
184 suppressed in *daf-2; daf-16* and *daf-7; daf-3* double mutants ***(Figure 3A, B).*** Therefore, it is
185 likely that insulin and TGF-β signaling modulate H_2S responses by regulating the expression
186 of relevant genes via DAF-16 and DAF-3 transcription factors, respectively. Given that H_2S-
187 evoked speed response was modulated by the nutrient-sensitive pathways, we further explored
188 whether the locomotory response to H_2S was sensitive to the nutrient state. Similar to the
189 response to CO_2 (Bretscher et al., 2008; Hallem & Sternberg, 2008), we observed that a 24-
190 hour period of starvation suppressed the speed response to H_2S ***(Figure 3D).*** However, the CO_2
191 sensor GCY-9 was dispensable for H_2S-evoked avoidance ***(Figure 3—figure supplement 1G–***
192 ***I).*** These findings suggest that even though acute avoidance of CO_2 and H_2S are modulated
193 through shared mechanisms, distinct molecular sensors are used.
194
195 **The O_2 sensing circuit antagonizes H_2S avoidance in wild isolates**
196 Wild strains of *C. elegans* thrive in environmental niches characterized by variable O_2, CO_2
197 and H_2S levels (Adams et al., 1979; Bretscher et al., 2008; Budde & Roth, 2011; Gea, Barrena,
198 Artola, & Sanchez, 2004; Hallem & Sternberg, 2008; Morra & Dick, 1991; Oshins, Michel,
199 Louis, Richard, & Rynk, 2022; Patange et al., 2025; Rodriguez-Kabana et al., 1965). Compared
200 to the laboratory reference strain N2, wild isolates display robust responses to high O_2 but
201 reduced sensitivity to CO_2 stimulation (Beets et al., 2020; Bretscher et al., 2008; Carrillo,
202 Guillermin, Rengarajan, Okubo, & Hallem, 2013; Hallem & Sternberg, 2008; Kodama-Namba
203 et al., 2013; McGrath et al., 2009). It is thought that the unique O_2 and CO_2 responses of N2
204 strain evolved during its domestication on solid media at atmospheric gas concentrations

205 (Sterken, Snoek, Kammenga, & Andersen, 2015). We hypothesized that wild *C. elegans* strains
206 might also exhibit an attenuated response to H_2S, and therefore included a set of wild strains in
207 our candidate gene screen. Consistent with this hypothesis, wild isolates including CB4855,
208 CB4856, and CB4858 exhibited reduced locomotory speed in H_2S (***Figure 3E, Figure 3—***
209 ***figure supplement 1J***).

210 A naturally occurring variation in the neuropeptide receptor NPR-1 predominantly
211 determines the differences in locomotory responses to O_2 and CO_2 between the laboratory N2
212 strain and wild isolates. The NPR-1(215F) variant found in wild isolates is less active than the
213 NPR-1(215V) found in N2 animals (de Bono & Bargmann, 1998). We wondered whether the
214 variations in the *npr-1* gene also contribute to differences in the acute response to H_2S. The
215 absence of *npr-1* was sufficient to reduce the speed response to H_2S, suggesting that active
216 NPR-1 signaling promotes H_2S avoidance (***Figure 3F***). NPR-1(215V) primarily acts within the
217 RMG interneurons to modulate responses to environmental stimuli by inhibiting signal output
218 from these neurons (***Figure 3G***) (Laurent et al., 2015; Macosko et al., 2009). Cell-specific
219 expression of the highly active *npr-1(215V)* variant in RMG neurons effectively restored the
220 H_2S-evoked locomotory speed in *npr-1* null mutant worms (***Figure 3H***). Furthermore,
221 optogenetic stimulation of RMG interneurons using channelrhodopsin-2 (ChR2) significantly
222 dampened the locomotory response to H_2S in N2 animals, suggesting that high RMG activity
223 inhibits H_2S responses (***Figure 3—figure supplement 1K***).

224 The perception of 21% O_2 involves the soluble guanylate cyclases GCY-35/GCY-36
225 and the downstream cyclic nucleotide-gated (CNG) channels TAX-4/TAX-2 in the URX, AQR,
226 and PQR O_2-sensing neurons, which relay the signals to RMG (Busch et al., 2012; Cheung,
227 Cohen, Rogers, Albayram, & de Bono, 2005; Couto, Oda, Nikolaev, Soltesz, & de Bono, 2013;
228 Gray et al., 2004; Laurent et al., 2015; Persson et al., 2009; Zimmer et al., 2009). We
229 investigated whether disrupting the O_2 sensing machinery would have the same effect as
230 inhibiting RMG signaling pathway by NPR-1(215V). Mutating *gcy-35* and *tax-4*, or genetically
231 ablating the O_2 sensing neurons URX, AQR, and PQR by cell-specific expression of the pro-
232 apoptotic gene *egl-1* restored H_2S-evoked speed response in *npr-1* null mutants (***Figure 3I–K***).

233 Specific expression of *gcy-35* cDNA in O_2 sensing neurons was sufficient to repress this
234 response to H_2S in *npr-1; gcy-35* double mutants (***Figure 3L***). Finally, enhancing the
235 presynaptic activity of URX, AQR, PQR neurons by the expression of a gain-of-function PKC-
236 1(A160E) (Dekker, Mcintyre, & Parker, 1993; Hiroki et al., 2022) significantly dampened H_2S-
237 induced locomotory speed (***Figure 3—figure supplement 1L***). Taken together, these
238 observations indicate that activation of the O_2-sensing circuit inhibits the H_2S-evoked
239 avoidance response.
240
241 **H_2S exposure reprograms gene expression in *C. elegans***
242 Wild isolates that were relatively insensitive to H_2S exposure (***Figure 3E, Figure 3—figure***
243 ***supplement 1J***) likely developed sensory and physiological adaptations to persist in
244 environments where H_2S may transiently increase (Budde & Roth, 2011; Patange et al., 2025;
245 Rodriguez-Kabana et al., 1965; Romanelli-Cedrez et al., 2024). These adaptations to H_2S are
246 mediated, at least in part, by the reprogramming of gene expression (Miller et al., 2011a). To
247 identify the genes whose expression was induced by prolonged H_2S exposure, we conducted a
248 comparative analysis of transcriptome profiles in animals exposed to 50 ppm or 150 ppm H_2S
249 for 1 hour, 2 hours, or 12 hours. RNA-seq analysis revealed that exposure to either 50 ppm or
250 150 ppm H_2S for one hour was sufficient to trigger significant changes in gene expression, with
251 518 or 304 genes showing differential expression, respectively (***Figure 4A, Supplementary file***
252 ***2***). Genes induced by H_2S exposure for 1 or 2 hours displayed considerable overlap (***Figure 4B,***
253 ***Figure 4—figure supplement 1A***). Gene Ontology (GO) analysis revealed that biological
254 processes such as defense against bacteria and cysteine biosynthesis from L-serine were
255 significantly enriched after H_2S exposure (***Figure 4C, D, Figure 4—figure supplement 1B, C***).
256 As expected, we observed a robust induction of genes involved in H_2S detoxification (***Figure***
257 ***4E, F***) (Miller, Budde, & Roth, 2011b; Niu et al., 2011; Vora et al., 2022). H_2S is detoxified in
258 mitochondria by sulfide:quinone oxidoreductase SQRD-1 to produce persulfide, which is then
259 metabolized by sulfur dioxygenase ETHE-1 to generate sulfite. Thiosulfate transferase further
260 oxidizes sulfite to produce thiosulfate (Hildebrandt & Grieshaber, 2008). Glutathione S-

261 transferases (GSTs) remove accumulated sulfur molecules during H_2S oxidation (Jackson,
262 Melideo, & Jorns, 2012). Notably, *gst-19* and *sqrd-1* were among the most significantly
263 upregulated genes after one or two hours of exposure to either 50 ppm or 150 ppm H_2S, while
264 *ethe-1* showed a weak increase (***Figure 4E, F, Figure 4—figure supplement 1D, E,***
265 ***Supplementary file 2***).

266 H_2S exposure is known to activate the HIF-1 pathway (Budde & Roth, 2010, 2011; Ma,
267 Vozdek, Bhatla, & Horvitz, 2012; Miller et al., 2011a; Miller & Roth, 2007; Vora et al., 2022).
268 In line with this, a proportion of genes with HIF-1 regulated promoters displayed increased
269 expression after 1 or 2 hours of H_2S exposure (***Figure 4—figure supplement 1F***). Among these
270 were the aforementioned detoxifying enzymes GST-19, SQRD-1, and ETHE-1, as well as
271 CYSL-1, CYSL-2, and CDO-1, which are involved in cysteine metabolism (***Supplementary***
272 ***file 2***). Consistent with earlier studies, we also observed differential expression of a set of SKN-
273 1 targets in response to chronic H_2S exposure (***Figure 4—figure supplement 1G***) (Horsman et
274 al., 2019; Miller et al., 2011a; Niu et al., 2011). This included the heat shock protein genes *hsp-*
275 *16.2* and *hsp-16.41* (***Figure 4E, F, Figure 4—figure supplement 1D, E***). Surprisingly, we
276 detected a rapid increase in the expression of genes associated with intracellular H_2S production,
277 including the methanethiol oxidase-encoding gene *semo-1* and the mercaptopyruvate
278 sulfurtransferase-encoding gene *mpst-3* (***Figure 4E, F, Figure 4—figure supplement 1D, E***)
279 (Philipp et al., 2022; Qabazard et al., 2014). Elevated expression of 3-mercaptopyruvate
280 sulfurtransferase has similarly been reported in sulfide spring fish, suggesting a conserved
281 response mechanism to H_2S (Kelley et al., 2016; Mathew, Schlipalius, & Ebert, 2011; Qabazard
282 et al., 2014). However, the functional implications of increased expression of H_2S synthesis
283 genes remains unclear.

284 When exposed to H_2S for 12 hours, the differentially expressed genes showed reduced
285 overlap with those identified at earlier time points (***Figure 4B, Figure 4—figure supplement***
286 ***1A***), suggesting that distinct defense strategies may be employed at various stages of H_2S
287 exposure. Furthermore, substantial overlap was observed between the sets of genes induced by
288 50 ppm and 150 ppm H_2S after 1h or 2h exposure. However, this overlap decreased

289 significantly after 12 hours exposure (***Figure 4—figure supplement 1H–J***). Additionally, we
290 noticed that 150 ppm H_2S specifically triggered the expression of the HIF-1 regulator *rhy-1* and
291 the HIF-1 target *nhr-57* at all exposure time points, a response that was less pronounced at 50
292 ppm H_2S (***Figures 4E, F, Figure 4—figure supplement 1D, E, K and L***). Together, these
293 findings suggest that multiple defense mechanisms are induced to adapt to the stress imposed
294 by H_2S, which can diverge over time and at different H_2S concentrations.
295
296 **Locomotory speed response to H_2S is modulated by HIF-1-induced detoxification**
297 Given that HIF-1 signaling is robustly activated shortly after H_2S exposure (***Figure 4—figure***
298 ***supplement 1F***) (Budde & Roth, 2010, 2011; Miller et al., 2011a), we next sought to determine
299 how HIF-1 signaling might contribute to H_2S-evoked avoidance response, and began by
300 examining the effects of HIF-1 stabilization. Acclimating animals in 1% O_2 for 12 hours or
301 longer significantly decreased the speed response to H_2S, indicating that HIF-1 stabilization
302 inhibits the H_2S-evoked avoidance behavior **(*Figure 5A*)**. To confirm this observation, we
303 examined several mutants with stabilized HIF-1. The conserved proline-4-hydroxylase
304 PHD/EGL-9 and the von Hippel-Lindau (VHL) tumor suppressor protein are required for HIF-
305 1 degradation (Kaelin & Ratcliffe, 2008; Semenza, 2010). Disruption of either *egl-9* or *vhl-1*
306 leads to HIF-1 stabilization under normoxic conditions. Similar to the effect of prolonged
307 hypoxia, both mutants exhibited a markedly reduced locomotory speed in H_2S **(*Figure 5B*).**
308 Interestingly, the omega-turn and reversal responses to H_2S were also substantially inhibited in
309 *egl-9* mutants **(*Figure 5—figure supplement 1A, B*)**. In contrast, the locomotory speed
310 response to 1% O_2 remained largely unaffected in *egl-9* deficient animals **(*Figure 5—figure***
311 ***supplement 1C*),** suggesting a selective impairment of the H_2S response. In addition, expressing
312 the non-degradable forms of HIF-1, *hif-1*(P621A or P621G), under the pan-neuronal *unc-14*
313 promoter or under the endogenous *hif-1* promoter, was sufficient to inhibit H_2S evoked speed
314 responses (***Figure 5C***). Together, these findings indicate that the activation of HIF-1 signaling
315 during prolonged H_2S or hypoxia exposure mediates an adaptive response associated with

316 reduced behavioral responses to H_2S, and that HIF-1 stabilization in neurons alone is sufficient
317 to promote this behavioral adaptation.

318 On the other hand, animals lacking HIF-1 signaling have previously been shown to
319 display increased sensitivity to H_2S and become paralyzed rapidly upon exposure (Budde &
320 Roth, 2010; Horsman et al., 2019). Consistent with this, *hif-1* mutants exhibited a brief increase
321 in speed upon H_2S exposure, which rapidly declined to baseline levels (***Figure 5D***). They also
322 displayed a stronger initial omega-turn response and greater inhibition of the reversal rate than
323 WT (***Figure 5E, F***), confirming that animals deficient in HIF-1 signaling are sensitized to H_2S
324 exposure. This transient avoidance behavior was also observed in *egl-9; hif-1* and *vhl-1; hif-1*
325 double mutants (***Figure 5G, H***), suggesting that this phenotype is linked to the absence of HIF-
326 1 signaling. Importantly, *hif-1* mutants displayed a robust speed response to other stimuli, such
327 as near-UV light and 1% O_2 stimulation ***(Figure 5I, Figure5—figure supplement 1D)***,
328 suggesting that the brief avoidance response is specific to H_2S rather than reflecting a general
329 locomotory defect. Further supporting increased sensitivity to H_2S in *hif-1* mutants, the
330 locomotory speed response of *hif-1* mutants to subsequent near-UV light stimulation was nearly
331 abolished after 30 minutes of H_2S exposure, whereas *egl-9* mutants and WT animals remained
332 fully responsive ***(Figure 5I)***. The reduced movement and lack of responsiveness to other
333 stressors in *hif-1* mutants resemble the stress-induced sleep-like behavior previously observed
334 in response to noxious heat (Byrne Rodgers & Ryu, 2020). Prompted by this observation, we
335 next explored whether HIF-1-induced detoxification genes were also required to maintain H_2S-
336 evoked behavioral responses (***Figure 5—figure supplement 1E)***. Similar to *hif-1* mutants,
337 *sqrd-1* and *ethe-1* mutants displayed brief responses to H_2S, with locomotory activity rapidly
338 returning to baseline levels ***(Figure 5J, K, Figure 5—figure supplement 1F–I)***. However, both
339 mutants responded normally to 1% O_2, suggesting a specific hypersensitivity to H_2S toxicity
340 ***(Figure 5—figure supplement 1J).*** Furthermore, we examined the contribution of additional
341 genes whose expression was upregulated in response to H_2S, including the
342 sulfhydrylase/cysteine synthase-encoding genes *cysl-1*, *cysl-2*, and *cysl-3*, as well as *semo-1*.
343 Disrupting any of these genes phenocopied the responses observed in *hif-1, ethe-1*, or *sqrd-1*

344 mutants, while they displayed normal responses to 1% O_2 (***Figure 5L, Figure 5—figure***
345 ***supplement 1D, K–P***). These observations suggest that while the HIF-1-induced H_2S
346 detoxification system is not essential for the initial sensing of H_2S, it is required to maintain
347 animals' locomotory activity in the presence of H_2S.
348
349 **Labile iron pool sustains the locomotory activity in H_2S**
350 Among the most differentially regulated genes upon exposure to H_2S, we observed consistent
351 downregulation of *ftn-1* and to a lesser extent *ftn-2*, whereas *smf-3* expression was increased
352 under specific H_2S conditions (***Figure 6A, B, Figure 6—figure supplement 1A–D***). The
353 ferritin-encoding genes *ftn-1* and *ftn-2,* along with the iron transporter *smf-3*, are critical for
354 maintaining intracellular labile iron homeostasis in *C. elegans* (Ackerman & Gems, 2012;
355 Gourley, Parker, Jones, Zumbrennen, & Leibold, 2003; Rajan et al., 2019; Romney, Newman,
356 Thacker, & Leibold, 2011), suggesting that H_2S exposure may interfere with cellular iron
357 storage. It has been shown that disrupting *ftn-1* increases labile iron pools in the cytoplasm,
358 while its overexpression reduces these levels (Anderson & Leibold, 2014; Romney et al., 2011).
359 We found that *ftn-1* mutants had enhanced speed response to H_2S, whereas *ftn-1* overexpression
360 attenuated H_2S-induced speed increase without damaging acute response to 1% O_2 (***Figure 6C,***
361 ***D, Figure 6—figure supplement 1E)***. In addition, *smf-3* mutants, which impair iron uptake,
362 exhibited a reduced speed response to H_2S (***Figure 6D***). These results support the idea that H_2S
363 exposure disrupts iron homeostasis.
364 To complement our genetic analysis, we pharmacologically depleted labile irons. In
365 the presence of the iron chelator 2,2'-dipyridyl (BP), the H_2S-evoked speed response was fully
366 lost (***Figure 6E***), whereas locomotory speed in response to hypoxia was maintained (***Figure***
367 ***6—figure supplement 1F).*** We noticed that, similar to *hif-1* mutants, both *smf-3* mutants and
368 BP-treated animals exhibited a strong initial omega-turn response to H_2S (***Figure 6—figure***
369 ***supplement 1G, I)***, suggesting that these animals are hypersensitive to H_2S toxicity. One
370 possibility is that low iron levels compromise H_2S detoxification capacity, as the detoxification
371 enzyme ETHE-1 requires iron for its activity (Kabil & Banerjee, 2012; Pettinati, Brem,

372 McDonough, & Schofield, 2015). By contrast, increasing iron levels by feeding ferric
373 ammonium citrate (FAC) or by disrupting *ftn-1* significantly sustained animals' locomotory
374 speed in H_2S (***Figure 6D, E***), likely by delaying H_2S-mediated iron depletion. However, the
375 reorientation and reversals were not significantly affected (***Figure 6—figure supplement 1G–***
376 ***J***). This impact of FAC supplementation and *ftn-1* disruption on speed response was largely
377 lost in the absence of *hif-1* (***Figure 6F, G***), suggesting that the effects of iron require HIF-1-
378 dependent detoxification (***Figure 6H)***. Yet, increased iron availability modestly improved the
379 locomotory activity of *hif-1* mutants in H_2S (***Figure 6F, G***), presumably by compensating for
380 the low iron levels in *hif-1* mutant animals (Rajan et al., 2019; Romney et al., 2011).
381
382 **Mitochondrial function modulates H_2S-evoked locomotion responses**
383 The mitochondrial electron transport chain (ETC) is not only the primary target of H_2S
384 toxicity, but is also an essential component of the H_2S detoxification pathways (Cooper &
385 Brown, 2008; Khan et al., 1990; Nicholls & Kim, 1982; Romanelli-Cedrez et al., 2024).
386 Based on this, we hypothesized that ETC plays a central role in the locomotory response to
387 H_2S. Indeed, mutating the genes critical for ETC function, including *gas-1*, *clk-1*, *mev-1,* and
388 *isp-1*, impaired the H_2S-evocked speed and reversal responses (***Figure 7A–D, Figure 7—***
389 ***figure supplement 1A–D)***. These data suggest that a functional ETC is required to trigger and
390 support H_2S-evoked avoidance behavior or that dysfunctional ETC induces an adaptive
391 response to cellular stressors. Consistently, exposing animals to rotenone, an ETC complex I
392 inhibitor, robustly inhibited the speed responses to H_2S at all time points we tested (***Figure***
393 ***7E***). Interestingly, we noticed that transient rotenone exposure substantially increased
394 animals' basal locomotory speed (***Figure 7E***) (Onukwufor et al., 2022), suggesting that acute
395 ETC interruption evokes behavioral avoidance, in a manner similar to that observed with
396 other noxious stimuli. However, a 2-hour exposure to rotenone abolished the H_2S-evocked
397 speed response without increasing the basal locomotory speed (***Figure 7E***), suggesting that
398 prolonged ETC inhibition may either impair the cellular capacity to support H_2S-evoked

399 behavioral responses or drive animals' adaptation to cellular stress and consequently reduce
400 their locomotory response to H_2S.
401 Given that rotenone exposure and mutations in ETC genes increase mitochondrial
402 ROS generation (Ishii et al., 2013; Ochi et al., 2016; Ramsay & Singer, 1992; Yang &
403 Hekimi, 2010; Zorov, Juhaszova, & Sollott, 2014), and that high levels of H_2S also induce
404 ROS production (Jia et al., 2020), we sought to determine how mitochondrial ROS
405 contributes to speed response to high H_2S. We focused on superoxide dismutases (SODs), key
406 enzymes in superoxide detoxification. The *C. elegans* genome encodes five *sod* genes: *sod-1*
407 and *sod-5* encode cytosolic Cu/ZnSODs, *sod-2* and *sod-3* encode mitochondrial MnSODs,
408 and *sod-4* encodes the extracellular Cu/ZnSOD isoforms (Doonan et al., 2008; Zubovych,
409 Straud, & Roth, 2010). All *sod* single mutants exhibited a robust initial response to 150 ppm
410 H_2S ***(Figure 7F, G).*** Interestingly, the mitochondrial SOD mutants *sod-2* and *sod-3*, as well
411 as *sod-5*, showed an initial burst of locomotory activity followed by a rapid decline in speed
412 in the presence of H_2S ***(Figure 7F, G)***, but maintained a high locomotory speed in response to
413 1% O_2 ***(Figure 7—figure supplement 1E)***. In the quintuple *sod-1; sod-2; sod-3; sod-4; sod-5*
414 mutant, which lacks all superoxide dismutases and presumably accumulates higher ROS
415 levels, the H_2S-evoked speed and omega-turn responses were nearly abolished, and the
416 proportion of animals exhibiting reversals remained consistently high, a pattern resembling
417 that of *egl-9* and ETC mutants ***(Figure 7G, Figure 7—figure supplement 1F, G)***. Similar to
418 *sod-2* and *sod-3*, the quintuple *sod* mutant exhibited robust speed response to 1% O_2 (Zhao et
419 al., 2022). In addition, the quintuple mutants responded normally to near-UV light after 30
420 minutes of H_2S exposure (***Figure 7—figure supplement 1H)***, indicating that their
421 neuromuscular function remains largely preserved. Therefore, high ROS levels in *sod* mutants
422 do not substantially compromise the detoxification capacity required for survival in H_2S.
423 Instead, high ROS appears to promote adaptation to H_2S-induced stress, presumably by
424 activating several stress-responsive pathways such as HIF-1, NRF2/SKN-1, and DAF-
425 16/FOXO (***Figure 7H***) (Lennicke & Cocheme, 2021; Patten, Germain, Kelly, & Slack, 2010).
426

427 **Discussion**

428 Animals' behavior and physiology are profoundly influenced by the environments in which
429 they evolved. The laboratory strain N2, which is adapted to low atmospheric CO_2 and H_2S
430 concentrations, robustly avoids both gases (Beets et al., 2020; Bretscher et al., 2008; Carrillo
431 et al., 2013; Hallem & Sternberg, 2008; Kodama-Namba et al., 2013; McGrath et al., 2009).
432 Upon acute exposure to H_2S above 75 ppm, N2 exhibits an avoidance behavior characterized
433 by reorientation and increased locomotion. This response is significantly reduced in wild
434 isolates. These divergent responses between the laboratory strain and wild isolates are primarily
435 driven by variations in the *npr-1* gene, which encodes a neuropeptide receptor, suggesting that
436 *C. elegans* has undergone rapid evolutionary adaptation to its environment.

437 The behavioral response to a specific sensory stimulus is usually shaped by an interplay
438 of multiple environmental and physiological cues. We observe that conditions dampening *C.*
439 *elegans'* response to CO_2 also impair the response to H_2S. Specifically, the speed response to
440 H_2S is significantly inhibited at high O_2 levels, and in mutants with defective insulin or TGF-β
441 pathway that signal starvation. However, despite these shared modulation, CO_2 and H_2S sensing
442 involve distinct molecular mechanisms. For example, CO_2 responses are mediated by the
443 guanylate cyclase GCY-9 in BAG neurons (Hallem et al., 2011), which is dispensable for H_2S
444 sensing. In addition, acute exposure to H_2S induces stronger reorientation but delayed
445 acceleration compared to CO_2, suggesting different sensing and information processing
446 mechanisms (Bretscher et al., 2008). Therefore, even though responses to CO_2 and H_2S are
447 modulated by overlapping regulatory mechanisms, the two gases are detected by distinct
448 sensors and processed differently.

449 In a candidate gene survey, we excluded the potential involvement of globins, K^+
450 channels, biogenic amines, and most guanylate cyclases in H_2S responses. However, we
451 observed that H_2S avoidance requires the activity of guanylate cyclase DAF-11 in ASJ neurons,
452 as well as neurosecretion from these neurons. Since the DAF-11 pathway and neurosecretion
453 from ASJ neurons regulate developmental programs that modify sensory functions in *C.*
454 *elegans* (Murakami, Koga, & Ohshima, 2001), it is not surprising that *daf-11* mutants display

455 pleiotropic phenotypes including impaired H_2S and CO_2 responses (Hallem & Sternberg, 2008).
456 In addition, we did not detect an H_2S-evoked calcium transient in ASJ neurons. Therefore,
457 although ASJ neurons and DAF-11 activity are clearly required, the exact sensory neurons,
458 circuits, and molecular triggers mediating acute H_2S avoidance remain to be elucidated.

459 Consistent with previous reports (Horsman et al., 2019; Miller et al., 2011a), H_2S
460 exposure substantially alters the gene expression in *C. elegans*, including those involved in H_2S
461 detoxification and iron homeostasis pathways. The repression of *ftn-1* and induction of *smf-3*
462 observed during H_2S exposure suggest that H_2S depletes intracellular labile iron. Iron is a
463 critical cofactor required for the activity of many enzymes and supports a wide range of cellular
464 processes (Dev & Babitt, 2017; Hentze, Muckenthaler, & Andrews, 2004). One important
465 enzyme that requires labile iron as cofactor is PHD/EGL-9, which targets HIF-1 for degradation.
466 Changes in iron availability are therefore expected to modulate EGL-9 activity, which in turn
467 alter the expression of HIF-1-regulated genes (Liochev, 1996; Myllyharju & Kivirikko, 1997;
468 Read, Bentley, Archer, & Dunham-Snary, 2021; Xu & Moller, 2011). However, ETHE-1, a
469 key H_2S detoxification enzyme upregulated upon HIF-1 stabilization, also requires iron for its
470 persulfide dioxygenase activity (Kabil & Banerjee, 2012; Pettinati et al., 2015). Therefore, H_2S-
471 evoked responses under varying iron availability are determined by the combined effects of
472 labile iron on HIF-1 signaling and on the H_2S detoxification enzymes, among other factors. For
473 instance, although reduced iron availability in *smf-3* or BP-treated animals may promote the
474 HIF-1 induced detoxification pathways by inactivating EGL-9, the actual enzymatic clearance
475 of H_2S is impaired due to low ETHE-1 activity. Supporting this, *smf-3* mutants and BP-treated
476 animals display increased sensitivity to H_2S, including enhanced initial omega-turn responses
477 and rapid inhibition of locomotion. In contrast, increased iron availability in *ftn-1* mutants or
478 FAC-treated animals likely delays iron depletion during H_2S exposure, preserving ETHE-1
479 detoxification capacity and postponing the onset of HIF-1-mediated adaptations that are
480 associated with reduced locomotion. This may explain the sustained high locomotory speed
481 observed in *ftn-1* mutants or FAC-treated animals. In the absence of HIF-1, iron
482 supplementation only partially improves the locomotory response to H_2S, likely because the

483 H_2S detoxification system including ETHE-1 cannot be transcriptionally induced. The modest
484 effect observed may instead reflect correction of iron deficiency in *hif-1* mutants.

485 At concentrations below 50 ppm, H_2S is well tolerated or even preferred, with
486 beneficial effects such as improved thermotolerance (Budde & Roth, 2010; Fawcett et al., 2015;
487 Horsman et al., 2019; Miller & Roth, 2007; Qabazard et al., 2014). Notably, behavioral
488 avoidance is absent below 50 ppm H_2S, suggesting that escape behavior is triggered only when
489 H_2S is not efficiently detoxified. This led us to hypothesize that animals with enhanced
490 detoxification capacity would show reduced avoidance of otherwise toxic H_2S levels. Indeed,
491 the speed response to H_2S is attenuated when the detoxification program is upregulated under
492 conditions of constitutive activation of HIF-1, such as in *egl-9* or *vhl-1* mutants, after prolonged
493 exposure to 1% O_2, or when HIF-1 signaling is specifically activated in neurons. These
494 observations support the idea that the initial avoidance response to H_2S is likely driven by acute
495 toxicity, while the subsequent decline in speed reflects a rapid activation of adaptive
496 mechanisms, particularly through stabilization of HIF-1. The fact that wild type animals remain
497 responsive to other stimuli after prolonged H_2S exposure suggests that reduced locomotory
498 speed in H_2S reflects active desensitization rather than general paralysis. However, persistently
499 high H_2S exposure is likely to exhaust cellular defense systems, leading to toxicity and paralysis.
500 By contrast, the rapid loss of locomotion observed in *hif-1* mutants and detoxification-defective
501 mutants is mediated by a mechanism distinct from adaptation. Their loss of responsiveness to
502 other stimuli after H_2S exposure suggests that these animals likely become sensitized and
503 rapidly intoxicated by H_2S due to impaired detoxification. Therefore, H_2S exposure promotes
504 a behavioral program that includes an initial reorientation and acceleration responses followed
505 by a progressive adaptation driven by cellular detoxification processes. A similar behavioral
506 program has been observed in *C. elegans* during noxious heat exposure, which induces short-
507 term heat avoidance followed by long-lasting cytoprotective adaptation and a gradual reduction
508 in avoidance (Byrne Rodgers & Ryu, 2020).

509 The interaction of H_2S with mitochondrial ETC is multifaceted, acting as an electron
510 donor at low concentrations and becoming a potent toxicant at high levels (Szabo et al., 2014),

511 in part by promoting superoxide generation through complex IV inhibition and reverse electron
512 transport at complex I (Cooper & Brown, 2008; Jia et al., 2020; Khan et al., 1990; Nicholls &
513 Kim, 1982; Romanelli-Cedrez et al., 2024). We propose that mitochondria play a dual role in
514 H_2S-evoked locomotory avoidance. On one hand, the mitochondrial ETC contributes to H_2S
515 detoxification and promotes adaptation. On the other hand, toxic levels of H_2S remodel the
516 ETC, leading to increased ROS production, which may serve as a trigger for the avoidance
517 response. Supporting the idea that acute mitochondrial ROS generation initiates avoidance of
518 high H_2S levels, short-term rotenone exposure, known to promote mitochondrial ROS
519 formation (Ochi et al., 2016; Ramsay & Singer, 1992; Zorov et al., 2014), substantially
520 increases locomotory speed (Onukwufor et al., 2022). Meanwhile, the speed response to high
521 H_2S is fully suppressed by rotenone. This inhibition could result either from excessive
522 mitochondrial ROS generated by rotenone, which may dampen the H_2S-triggered ROS spike,
523 or from direct complex I inhibition, which may disrupt other H_2S signaling processes required
524 to initiate avoidance. However, persistent mitochondrial ROS production appears to suppress
525 high locomotory speed and inhibit responsiveness to H_2S, as observed after 2-hour rotenone
526 exposure, in mitochondrial ETC mutants, and in animals lacking all superoxide dismutases.
527 One likely explanation is that mitochondrial ROS can activate a variety of stress-responsive
528 pathways, including HIF-1, NRF2/SKN-1, and DAF-16/ FOXO signaling (Lennicke &
529 Cocheme, 2021; Patten et al., 2010), priming animals' adaptation to prolonged stress rather
530 than causing toxicity. This is supported by the observation that even though SOD-deficient
531 animals do not display strong initial locomotory responses to H_2S, they remain responsive to
532 other stimuli after 30 minutes of H_2S exposure, suggesting that high ROS levels do not
533 compromise general viability or the H_2S detoxification capacity. Therefore, we favor a model
534 in which mitochondrial ROS exert a biphasic effect on H_2S-induced avoidance, facilitating H_2S
535 detection and avoidance under acute conditions, and contributing to locomotory inhibition
536 when it is chronically elevated.

537 In summary, this study unveils a novel behavior of *C. elegans* in their avoidance to
538 H_2S. The speed response to H_2S is intricately shaped by environmental context, integrating

539 inputs from other sensory cues such as food availability and O_2 levels. Although we did not
540 identify the specific neural circuit mediating H_2S signaling, our findings suggest that H_2S-
541 induced locomotion arises from acute remodeling of mitochondrial ETC and mitochondrial
542 ROS production. We emphasize the vital role of the HIF-1-induced detoxification pathways
543 and iron homeostasis in protecting against H_2S-induced mitochondrial toxicity. In future work,
544 it will be important to delineate the neural circuits underlying H_2S-evoked locomotory
545 avoidance and to clarify how H_2S-induced changes in mitochondrial respiration and labile iron
546 pools shape these responses.
547

548 **Materials and Methods**

549 **Strains**

550 *C. elegans* were maintained using standard protocols (Brenner, 1974). Strains used in this study
551 are listed in ***Supplementary file 1*** and ***Supplementary file 3***.
552

553 **Preparation of H_2S gas mixture**

554 Different H_2S concentrations were created as previously described (Miller & Roth, 2007).
555 Briefly, the H_2S-containing gas mixture were prepared by diluting 5000 ppm H_2S in nitrogen
556 (N_2) with 7% O_2 balanced with N_2. The gas flow was tuned by Sierra Smart-Trak 100 mass
557 flow controllers. H_2S concentration in the mixture was measured using two H_2S detectors (MSA
558 ALTAIR 2X gas detector for H_2S and Clip Single Gas Detector, SDG, CROWCON). The pre-
559 defined gas mixtures of 7% O_2, 1% O_2 and 5% CO_2 with N_2 were purchased from Air Liquide
560 Gas AB. 5000 ppm H_2S stock in N_2 was obtained from Linde Gas AB. Gas mixtures in all
561 experiments were hydrated before use.
562

563 **Molecular Biology**

564 The Multisite Gateway system (Thermo Fisher Scientific, United States) was used to generate
565 expression vectors. Promoters, including *gcy-37* (2.7kb), *trx-1* (1 kb), *ftn-1*(2 kb), *daf-11*(3 kb),
566 *odr-3*(2.7 kb), *gpa-11*(3 kb), *sra-6*(3 kb), *odr-1*(2.4 kb), *flp-21*(4.1kb), and *ocr-2*(2.4 kb) were

567 amplified from N2 genomic DNA and cloned into pDONR P4P1 using BP clonase. g*cy-35*,
568 *tax-4,* and *pkc-1* cDNAs were amplified using the first strand cDNA library as the template,
569 while *daf-11* and *ftn-1* genomic sequences were amplified using genomic DNA as the template.
570 The entry clones of these genes pDONR 221 were generated using BP reaction. To generate
571 the gain of function mutation of *pkc-1* (A160E), Q5 Site-Directed Mutagenesis Kit (NEB) was
572 used according to manufacturer instructions. All expression vectors were generated using LR
573 reaction. The primer sequences were displayed in ***Supplementary file 4***.
574 To generate transgenic animals, the *daf-11* expression vectors were injected at the
575 concentration of 20 ng/µl supplemented with 50 ng/µl of a coelomocyte co-injection marker
576 (*unc-122p::GFP)* and 30 ng/µl of 1kb DNA ladder. For *tax-4* gene, the injection mixtures were
577 prepared using 40 ng/µl of *tax-4* expression vectors, 50 ng/µl of a coelomocyte co-injection
578 marker and 10 ng/µl of 1kb DNA ladder. The rest of expression constructs were injected at 50
579 ng/µl together with 50 ng/µl of a coelomocyte marker.
580
581 **CRISPR/Cas9 genome editing**
582 Genes were disrupted using CRISPR/Cas9 mediated genome editing as described (Dokshin,
583 Ghanta, Piscopo, & Mello, 2018; Ghanta & Mello, 2020). The strategy involved the utilization
584 of homology-directed insertion of custom designed single strand DNA template (ssODN),
585 which had two homology arms of 35bp flanking the targeted PAM site. Between two homology
586 arms, a short sequence containing a unique restriction enzyme cutting site as well as in-frame
587 and out-of-frame stop codons, was included. The insertion of ssODN template would delete 16
588 bases of coding sequence, ensuring the proper gene disruption. To prepare the injection cocktail,
589 0.5 µl of Cas9 protein (IDT) was mixed with 5 µl of 0.4µg/µl tracrRNA (IDT, United States)
590 and 2.8 µl of 0.4 µg/µl crRNA (IDT). The mixture was incubated at 37°C for at least 10 minutes
591 before 2.2 µl of 1µg/µl ssODN (or 500 ng dsDNA) and 2 µl of 0.6 µg/µl *rol-6* co-injection
592 marker were added. Nuclease-free water was used to bring the final volume to 20 µl. The
593 injection mixture was centrifuged for 2 minutes before use.
594

595 **Behavioral assays**

596 H_2S evoked locomotion activity was monitored as described previously (Laurent et al., 2015;
597 Zhao et al., 2022). Briefly, OP50 bacteria were seeded on the assay plates 16 hours before use.
598 The border of bacterial lawn was removed using a PDMS stamp. For each assay, 25 to 30 day-
599 one adult animals were picked onto assay plates, allowed to settle down for 15 minutes, and
600 subsequently sealed within microfluidic chambers. A syringe pump (PHD 2000, Harvard
601 Apparatus) was employed to deliver gas mixtures into the microfluidic chamber at a constant
602 flow of 3 ml/min. The rapid switch between different gas mixtures were controlled by Telfon
603 valves coupled with ValveBank Perfusion Controller (AutoMate Scientific). The locomotory
604 activity at different gas mixtures were monitored using a high-resolution camera (FLIR)
605 mounted on a Zeiss Stemi 508 microscope. Videos were captured at a rate of 2 frames per
606 second, starting with a 2-minute recording in 7% O_2, followed by 10 or 11 minutes in H_2S, and
607 ending with 7% O_2. For the long-term recording in H_2S, video capture commenced with a 2-
608 minute period in 7% O_2, followed by a duration of 148 minutes in 150 ppm H_2S, and concluded
609 with a final 2-minute interval in 7% O_2. For each strain or condition, 3 to 4 replicates were
610 performed.

611 Near-UV light experiments were conducted to assess whether animals remained
612 responsive following a 30-minute incubation in 150 ppm H_2S balanced with 7% O_2. For each
613 experiment, 6-minute videos were recorded. The first 2 minutes captured the baseline
614 locomotion of the animals under white light, followed by 2 minutes of exposure to near-UV
615 light (435 nm, 0.7 mW/mm^2), and concluded with 2 minutes of white light. 3 to 4 replicates
616 were performed, with approximately 15 animals recorded per replicate.

617 The H_2S gradient experiment was performed in a PDMS chamber connected to a pump
618 delivering gas at 0.5 ml/min. To establish a gradient ranging from 150 ppm to 0 ppm H_2S, we
619 pumped 150 ppm H_2S balanced with 7% O_2 into one side and 7% O_2 into the opposite side.
620 After 25 minutes, the number of animals in each of the 5 sections was counted (***Figure 1G***).
621 Four replicates were performed, each using 30 day-one adult animals.

622 To assess the effects of rotenone on H_2S evoked locomotory response, day-one adult
623 animals were subjected to 10 μM rotenone for 10min, 30min, 1 hour and 2 hours on the drug
624 containing plates. Subsequently, the rotenone-treated animals were assayed on the standard
625 assay plates without the drug. To explore the impact of ferric ammonium citrate (FAC) (F5879,
626 Sigma-Aldrich) and 2,2′-Bipyridyl (BP) (D216305, Sigma-Aldrich) on behavioral response to
627 H_2S, L4 animals were exposed to 100 μM FAC or 5 mg/ml BP for 16 hours in the presence of
628 bacterial food. The FAC or BP treated animals were assayed on FAC or BP containing plates,
629 respectively.
630 Optogenetic experiments were performed as previously outlined (Zhao et al., 2022).
631 Transgenic L4 animals were exposed to 100 μM all-trans retinal (ATR) (R2500, Sigma) in the
632 dark for 16 hours. The ATR-fed animals were assayed with the illumination of 70 $\mu W/mm^2$
633 blue light during the whole assay period. Blue light was emitted from an ultra-high-power LED
634 lamp (UHP-MIC-LED-460, Prizmatix), and the light intensity was determined using a PM50
635 Optical Power Meter (ThorLabs). To minimize the effect of transmitted light on the transgenic
636 animals, a long-pass optical filter was used to eliminate the lights with short wavelengths during
637 picking. All videos of behavioral analysis were analyzed using a home-made MATLAB
638 program Zentracker (https://github.com/wormtracker/zentracker). For all behavior analyses, at
639 least three assays were performed for each strain with more than 80 worms in total.
640
641 **Ca^{2+} Imaging**
642 L4 animals expressing the GCaMP6s sensor in ASJ neurons were picked 24 hours before
643 imaging. The agarose pads were prepared 1 hour before the experiment. Animals were
644 incubated in 15 μl of 10 mM levamisole for 40 minutes prior to imaging. Between 15 and 20
645 animals were immobilized using 10 mM levamisole diluted in a concentrated OP50 bacterial
646 suspension and mounted on a 2% agarose pad in M9 buffer on a glass slide. The animals were
647 then covered with a microfluidic chamber. Imaging lasted for 16 minutes. O_2 (7%) was pumped
648 into the microfluidic chamber during the first and last 4 minutes. From minute 4 to 12, a mixture
649 of 7% O_2 and 150 ppm H_2S was pumped.

650 Imaging was performed on a Nikon AZ100 microscope equipped with a TwinCam
651 adapter (Cairn Research, UK), fitted with two DMK 33U monochrome cameras (The Imaging
652 Source, Germany). A 2x AZ Plan Fluor objective with 1x zoom was used, with an exposure
653 time of 300 ms. Excitation of GCaMP and RFP was provided by a CoolLED pE-300 (CoolLED,
654 UK). The TwinCam adapter was mounted with emission filters for green fluorescent protein
655 (510/20 nm) and red fluorescent protein (590/35 nm), along with a DC/T510LPXRXTUf2
656 dichroic mirror. Imaging data were analyzed using Neuron Analyzer, a custom-written Matlab
657 program for processing image stacks (code available at
658 https://github.com/neuronanalyser/neuronanalyser).
659
660 **RNA extraction and sequencing**
661 To obtain RNA samples for RNA-seq, thirty young adult animals were picked to each fresh
662 plate and allowed to lay eggs for 2 hours, after which the adult animals were removed and eggs
663 were allowed to develop into day-one adults. Day-one animals were subsequently challenged
664 with H_2S for three different time periods (1 hour, 2 hours and 12 hours). For each time period,
665 five plates of day-one animals were exposed to 50 ppm H_2S, 150 ppm H_2S or 7% O_2 as a control
666 group. Subsequently, the animals were immediately collected and rinsed three times with M9
667 buffer. After washing, the worm pellet was frozen in liquid nitrogen. Animals were
668 homogenized using Bullet Blender (Next Advance) in the presence of Qiazol Lysis Reagent
669 and 0.5mm Zirconia beads at 4°C. RNA was prepared using RNeasy Plus Universal Mini Kit
670 (Qiagen). Six independent RNA samples were prepared for each condition. The 2100
671 Bioanalyzer instrument (Agilent) was used for the RNA quality control with a microfluidic chip
672 specific for RNA (Agilent RNA 6000 Nano Kit). Then 1 μg of qualified RNA samples in
673 RNase-free ddH2O was used for library preparation. Library was constructed and sequenced
674 by Novogene.
675
676 **RNA-seq analysis**

677 The RNA-seq data were aligned using STAR v2.7.9a (Dobin et al., 2013) and gene expression
678 counts extracted by featureCounts v2.0.3 (Liao, Smyth, & Shi, 2014). Differential expression
679 was calculated using DESeq2 (Love, Huber, & Anders, 2014). GO analysis was performed
680 using the EnrichR R package (Kuleshov et al., 2016) on genes having *p*.adj < 1e-10. For brevity,
681 several highly similar GO categories were manually omitted (full EnrichR output available at
682 Github repository).
683
684 **Data availability**
685 Raw sequencing data has been deposited at ArrayExpress # E-MTAB-13296. The R code is
686 available at https://github.com/henriksson-lab/ce_h2s_tc.
687
688 **Acknowledgments**
689 We thank the Caenorhabditis Genetics Center (funded by NIH Office of Research Infrastructure
690 Programs P40 OD010440) and the National BioResources Project Japan for strains.
691
692 **Funding**
693 The computations were enabled by resources provided by the National Academic Infrastructure
694 for Supercomputing in Sweden (NAISS) and the Swedish National Infrastructure for
695 Computing (SNIC) at UPPMAX partially funded by the Swedish Research Council through
696 grant agreements no. 2022-06725 and no. 2018-05973. This work is supported by the Swedish
697 VR Research Council grant MIMS (2021-06602) to J.H., the Belgian National Fund for
698 Scientific Research (FRS-FNRS) to P.L., the ERC starting grant (802653 OXYGEN
699 SENSING), the Swedish Research Council VR starting grant (2018-02216), and the
700 Wallenberg Centre for Molecular Medicine (Umeå) to C.C.
701
702 **References**

Abel, D. C., Koenig, C. C., & Davis, W. P. (1987). Emersion in the Mangrove Forest Fish Rivulus-Marmoratus - a Unique Response to Hydrogen-Sulfide. *Environmental Biology of Fishes, 18*(1), 67-72. doi:Doi 10.1007/Bf00002329

Ackerman, D., & Gems, D. (2012). Insulin/IGF-1 and Hypoxia Signaling Act in Concert to Regulate Iron Homeostasis in *Caenorhabditis elegans*. *Plos Genetics, 8*(3). doi:ARTN e1002498
10.1371/journal.pgen.1002498

Adams, D. F., Farwell, S. O., Pack, M. R., & Bamesberger, W. L. (1979). Preliminary Measurements of Biogenic Sulfur-Containing Gas Emissions from Soils. *Journal of the Air Pollution Control Association, 29*(4), 380-383. doi:Doi 10.1080/00022470.1979.10470805

Anderson, C. P., & Leibold, E. A. (2014). Mechanisms of iron metabolism in *Caenorhabditis elegans*. *Frontiers in Pharmacology, 5*. doi:ARTN 113
10.3389/fphar.2014.00113

Beets, I., Zhang, G., Fenk, L. A., Chen, C., Nelson, G. M., Felix, M. A., & de Bono, M. (2020). Natural Variation in a Dendritic Scaffold Protein Remodels Experience-Dependent Plasticity by Altering Neuropeptide Expression. *Neuron, 105*(1), 106-121 e110. doi:10.1016/j.neuron.2019.10.001

Brenner, S. (1974). The genetics of *Caenorhabditis elegans*. *Genetics, 77*(1), 71-94. Retrieved from https://www.ncbi.nlm.nih.gov/pubmed/4366476

Bretscher, A. J., Busch, K. E., & de Bono, M. (2008). A carbon dioxide avoidance behavior is integrated with responses to ambient oxygen and food in *Caenorhabditis elegans*. *Proc Natl Acad Sci U S A, 105*(23), 8044-8049. doi:10.1073/pnas.0707607105

Budde, M. W., & Roth, M. B. (2010). Hydrogen sulfide increases hypoxia-inducible factor-1 activity independently of von Hippel-Lindau tumor suppressor-1 in *C. elegans*. *Mol Biol Cell, 21*(1), 212-217. doi:10.1091/mbc.E09-03-0199

729 Budde, M. W., & Roth, M. B. (2011). The response of *Caenorhabditis elegans* to hydrogen
730 sulfide and hydrogen cyanide. *Genetics, 189*(2), 521-532.
731 doi:10.1534/genetics.111.129841
732 Busch, K. E., Laurent, P., Soltesz, Z., Murphy, R. J., Faivre, O., Hedwig, B., . . . de Bono, M.
733 (2012). Tonic signaling from O(2) sensors sets neural circuit activity and behavioral
734 state. *Nat Neurosci, 15*(4), 581-591. doi:10.1038/nn.3061
735 Byrne Rodgers, J., & Ryu, W. S. (2020). Targeted thermal stimulation and high-content
736 phenotyping reveal that the *C. elegans* escape response integrates current behavioral
737 state and past experience. *PLoS One, 15*(3), e0229399.
738 doi:10.1371/journal.pone.0229399
739 Carrillo, M. A., Guillermin, M. L., Rengarajan, S., Okubo, R. P., & Hallem, E. A. (2013). O-
740 2-Sensing Neurons Control CO_2 Response in *C. elegans*. *Journal of Neuroscience,*
741 *33*(23), 9675-9683. doi:10.1523/Jneurosci.4541-12.2013
742 Chang, A. J., Chronis, N., Karow, D. S., Marletta, M. A., & Bargmann, C. I. (2006). A
743 distributed chemosensory circuit for oxygen preference in *C. elegans*. *PLoS Biol,*
744 *4*(9), e274. doi:10.1371/journal.pbio.0040274
745 Cheung, B. H., Cohen, M., Rogers, C., Albayram, O., & de Bono, M. (2005). Experience-
746 dependent modulation of *C. elegans* behavior by ambient oxygen. *Curr Biol, 15*(10),
747 905-917. doi:10.1016/j.cub.2005.04.017
748 Cooper, C. E., & Brown, G. C. (2008). The inhibition of mitochondrial cytochrome oxidase
749 by the gases carbon monoxide, nitric oxide, hydrogen cyanide and hydrogen sulfide:
750 chemical mechanism and physiological significance. *J Bioenerg Biomembr, 40*(5),
751 533-539. doi:10.1007/s10863-008-9166-6
752 Couto, A., Oda, S., Nikolaev, V. O., Soltesz, Z., & de Bono, M. (2013). In vivo genetic
753 dissection of O_2-evoked cGMP dynamics in a *Caenorhabditis elegans* gas sensor.
754 *Proc Natl Acad Sci U S A, 110*(35), E3301-3310. doi:10.1073/pnas.1217428110

755 de Bono, M., & Bargmann, C. I. (1998). Natural variation in a neuropeptide Y receptor
756 homolog modifies social behavior and food response in *C. elegans*. *Cell, 94*(5), 679-
757 689. doi:10.1016/s0092-8674(00)81609-8
758 Dekker, L. V., Mcintyre, P., & Parker, P. J. (1993). Mutagenesis of the Regulatory Domain of
759 Rat Protein Kinase-C-Eta - a Molecular-Basis for Restricted Histone Kinase-Activity.
760 *Journal of Biological Chemistry, 268*(26), 19498-19504. Retrieved from <Go to
761 ISI>://WOS:A1993LW81900055
762 Dev, S., & Babitt, J. L. (2017). Overview of iron metabolism in health and disease. *Hemodial*
763 *Int, 21 Suppl 1*(Suppl 1), S6-S20. doi:10.1111/hdi.12542
764 Dobin, A., Davis, C. A., Schlesinger, F., Drenkow, J., Zaleski, C., Jha, S., . . . Gingeras, T. R.
765 (2013). STAR: ultrafast universal RNA-seq aligner. *Bioinformatics, 29*(1), 15-21.
766 doi:10.1093/bioinformatics/bts635
767 Dokshin, G. A., Ghanta, K. S., Piscopo, K. M., & Mello, C. C. (2018). Robust Genome
768 Editing with Short Single-Stranded and Long, Partially Single-Stranded DNA Donors
769 in *Caenorhabditis elegans*. *Genetics, 210*(3), 781-787.
770 doi:10.1534/genetics.118.301532
771 Doonan, R., McElwee, J. J., Matthijssens, F., Walker, G. A., Houthoofd, K., Back, P., . . .
772 Gems, D. (2008). Against the oxidative damage theory of aging: superoxide
773 dismutases protect against oxidative stress but have little or no effect on life span in
774 *Caenorhabditis elegans*. *Genes Dev, 22*(23), 3236-3241. doi:10.1101/gad.504808
775 Fawcett, E. M., Hoyt, J. M., Johnson, J. K., & Miller, D. L. (2015). Hypoxia disrupts
776 proteostasis in *Caenorhabditis elegans*. *Aging Cell, 14*(1), 92-101.
777 doi:10.1111/acel.12301
778 Ferkey, D. M., Sengupta, P., & L'Etoile, N. D. (2021). Chemosensory signal transduction in
779 *Caenorhabditis elegans*. *Genetics, 217*(3). doi:10.1093/genetics/iyab004
780 Gao, L., Gonzalez-Rodriguez, P., Ortega-Saenz, P., & Lopez-Barneo, J. (2017). Redox
781 signaling in acute oxygen sensing. *Redox Biol, 12*, 908-915.
782 doi:10.1016/j.redox.2017.04.033

783 Gea, T., Barrena, R., Artola, A., & Sanchez, A. (2004). Monitoring the biological activity of
784 the composting process: Oxygen uptake rate (OUR), respirometric index (RI), and
785 respiratory quotient (RQ). *Biotechnol Bioeng, 88*(4), 520-527. doi:10.1002/bit.20281
786 Ghanta, K. S., & Mello, C. C. (2020). Melting dsDNA Donor Molecules Greatly Improves
787 Precision Genome Editing in *Caenorhabditis elegans*. *Genetics, 216*(3), 643-650.
788 doi:10.1534/genetics.120.303564
789 Gourley, B. L., Parker, S. B., Jones, B. J., Zumbrennen, K. B., & Leibold, E. A. (2003).
790 Cytosolic aconitase and ferritin are regulated by iron in *Caenorhabditis elegans*. *J*
791 *Biol Chem, 278*(5), 3227-3234. doi:10.1074/jbc.M210333200
792 Gray, J. M., Karow, D. S., Lu, H., Chang, A. J., Chang, J. S., Ellis, R. E., . . . Bargmann, C. I.
793 (2004). Oxygen sensation and social feeding mediated by a *C. elegans* guanylate
794 cyclase homologue. *Nature, 430*(6997), 317-322. doi:10.1038/nature02714
795 Hallem, E. A., Spencer, W. C., McWhirter, R. D., Zeller, G., Henz, S. R., Ratsch, G., . . .
796 Ringstad, N. (2011). Receptor-type guanylate cyclase is required for carbon dioxide
797 sensation by *Caenorhabditis elegans*. *Proc Natl Acad Sci U S A, 108*(1), 254-259.
798 doi:10.1073/pnas.1017354108
799 Hallem, E. A., & Sternberg, P. W. (2008). Acute carbon dioxide avoidance in *Caenorhabditis*
800 *elegans*. *Proc Natl Acad Sci U S A, 105*(23), 8038-8043.
801 doi:10.1073/pnas.0707469105
802 Heiman, M. G., & Shaham, S. (2009). DEX-1 and DYF-7 establish sensory dendrite length
803 by anchoring dendritic tips during cell migration. *Cell, 137*(2), 344-355.
804 doi:10.1016/j.cell.2009.01.057
805 Hentze, M. W., Muckenthaler, M. U., & Andrews, N. C. (2004). Balancing acts: molecular
806 control of mammalian iron metabolism. *Cell, 117*(3), 285-297. doi:10.1016/s0092-
807 8674(04)00343-5
808 Hildebrandt, T. M., & Grieshaber, M. K. (2008). Three enzymatic activities catalyze the
809 oxidation of sulfide to thiosulfate in mammalian and invertebrate mitochondria.
810 *FEBS J, 275*(13), 3352-3361. doi:10.1111/j.1742-4658.2008.06482.x

811 Hiroki, S., Yoshitane, H., Mitsui, H., Sato, H., Umatani, C., Kanda, S., . . . Iino, Y. (2022).
812 Molecular encoding and synaptic decoding of context during salt chemotaxis in *C.*
813 *elegans*. *Nature Communications, 13*(1). doi:ARTN 2928
814 10.1038/s41467-022-30279-7
815 Horsman, J. W., Heinis, F. I., & Miller, D. L. (2019). A Novel Mechanism To Prevent H2S
816 Toxicity in *Caenorhabditis elegans*. *Genetics, 213*(2), 481-490.
817 doi:10.1534/genetics.119.302326
818 Ishii, T., Miyazawa, M., Onouchi, H., Yasuda, K., Hartman, P. S., & Ishii, N. (2013). Model
819 animals for the study of oxidative stress from complex II. *Biochim Biophys Acta,*
820 *1827*(5), 588-597. doi:10.1016/j.bbabio.2012.10.016
821 Jackson, M. R., Melideo, S. L., & Jorns, M. S. (2012). Human sulfide:quinone oxidoreductase
822 catalyzes the first step in hydrogen sulfide metabolism and produces a sulfane sulfur
823 metabolite. *Biochemistry, 51*(34), 6804-6815. doi:10.1021/bi300778t
824 Jia, J., Wang, Z., Zhang, M., Huang, C., Song, Y., Xu, F., . . . Cheng, J. (2020). SQR
825 mediates therapeutic effects of H(2)S by targeting mitochondrial electron transport to
826 induce mitochondrial uncoupling. *Sci Adv, 6*(35), eaaz5752.
827 doi:10.1126/sciadv.aaz5752
828 Kabil, O., & Banerjee, R. (2012). Characterization of patient mutations in human persulfide
829 dioxygenase (ETHE1) involved in H_2S catabolism. *J Biol Chem, 287*(53), 44561-
830 44567. doi:10.1074/jbc.M112.407411
831 Kaelin, W. G., Jr., & Ratcliffe, P. J. (2008). Oxygen sensing by metazoans: the central role of
832 the HIF hydroxylase pathway. *Mol Cell, 30*(4), 393-402.
833 doi:10.1016/j.molcel.2008.04.009
834 Kelley, J. L., Arias-Rodriguez, L., Patacsil Martin, D., Yee, M. C., Bustamante, C. D., &
835 Tobler, M. (2016). Mechanisms Underlying Adaptation to Life in Hydrogen Sulfide-
836 Rich Environments. *Mol Biol Evol, 33*(6), 1419-1434. doi:10.1093/molbev/msw020
837 Khan, A. A., Schuler, M. M., Prior, M. G., Yong, S., Coppock, R. W., Florence, L. Z., &
838 Lillie, L. E. (1990). Effects of hydrogen sulfide exposure on lung mitochondrial

respiratory chain enzymes in rats. *Toxicol Appl Pharmacol, 103*(3), 482-490. doi:10.1016/0041-008x(90)90321-k

Kodama-Namba, E., Fenk, L. A., Bretscher, A. J., Gross, E., Busch, K. E., & de Bono, M. (2013). Cross-modulation of homeostatic responses to temperature, oxygen and carbon dioxide in *C. elegans*. *PLoS Genet, 9*(12), e1004011. doi:10.1371/journal.pgen.1004011

Kuleshov, M. V., Jones, M. R., Rouillard, A. D., Fernandez, N. F., Duan, Q. N., Wang, Z. C., . . . Ma'ayan, A. (2016). Enrichr: a comprehensive gene set enrichment analysis web server 2016 update. *Nucleic Acids Research, 44*(W1), W90-W97. doi:10.1093/nar/gkw377

Laurent, P., Soltesz, Z., Nelson, G. M., Chen, C., Arellano-Carbajal, F., Levy, E., & de Bono, M. (2015). Decoding a neural circuit controlling global animal state in *C. elegans*. *Elife, 4*. doi:10.7554/eLife.04241

Lennicke, C., & Cocheme, H. M. (2021). Redox metabolism: ROS as specific molecular regulators of cell signaling and function. *Mol Cell, 81*(18), 3691-3707. doi:10.1016/j.molcel.2021.08.018

Liao, Y., Smyth, G. K., & Shi, W. (2014). featureCounts: an efficient general purpose program for assigning sequence reads to genomic features. *Bioinformatics, 30*(7), 923-930. doi:10.1093/bioinformatics/btt656

Liochev, S. L. (1996). The role of iron-sulfur clusters in in vivo hydroxyl radical production. *Free Radical Research, 25*(5), 369-384. doi:Doi 10.3109/10715769609149059

Love, M. I., Huber, W., & Anders, S. (2014). Moderated estimation of fold change and dispersion for RNA-seq data with DESeq2. *Genome Biology, 15*(12). doi:ARTN 550 10.1186/s13059-014-0550-8

Ma, D. K., Vozdek, R., Bhatla, N., & Horvitz, H. R. (2012). CYSL-1 interacts with the O_2-sensing hydroxylase EGL-9 to promote H_2S-modulated hypoxia-induced behavioral plasticity in *C. elegans*. *Neuron, 73*(5), 925-940. doi:10.1016/j.neuron.2011.12.037

866 Macosko, E. Z., Pokala, N., Feinberg, E. H., Chalasani, S. H., Butcher, R. A., Clardy, J., &
867 Bargmann, C. I. (2009). A hub-and-spoke circuit drives pheromone attraction and
868 social behaviour in *C. elegans*. *Nature, 458*(7242), 1171-1175.
869 doi:10.1038/nature07886
870 Mathew, N. D., Schlipalius, D. I., & Ebert, P. R. (2011). Sulfurous gases as biological
871 messengers and toxins: comparative genetics of their metabolism in model
872 organisms. *J Toxicol, 2011*, 394970. doi:10.1155/2011/394970
873 McGrath, P. T., Rockman, M. V., Zimmer, M., Jang, H., Macosko, E. Z., Kruglyak, L., &
874 Bargmann, C. I. (2009). Quantitative mapping of a digenic behavioral trait implicates
875 globin variation in *C. elegans* sensory behaviors. *Neuron, 61*(5), 692-699.
876 doi:10.1016/j.neuron.2009.02.012
877 Miller, D. L., Budde, M. W., & Roth, M. B. (2011a). HIF-1 and SKN-1 Coordinate the
878 Transcriptional Response to Hydrogen Sulfide in *Caenorhabditis elegans*. *PLoS One,*
879 *6*(9). doi:ARTN e25476
880 10.1371/journal.pone.0025476
881 Miller, D. L., Budde, M. W., & Roth, M. B. (2011b). HIF-1 and SKN-1 coordinate the
882 transcriptional response to hydrogen sulfide in *Caenorhabditis elegans*. *PLoS One,*
883 *6*(9), e25476. doi:10.1371/journal.pone.0025476
884 Miller, D. L., & Roth, M. B. (2007). Hydrogen sulfide increases thermotolerance and lifespan
885 in *Caenorhabditis elegans*. *Proc Natl Acad Sci U S A, 104*(51), 20618-20622.
886 doi:10.1073/pnas.0710191104
887 Morra, M. J., & Dick, W. A. (1991). Mechanisms of h(2)s production from cysteine and
888 cystine by microorganisms isolated from soil by selective enrichment. *Appl Environ*
889 *Microbiol, 57*(5), 1413-1417. doi:10.1128/aem.57.5.1413-1417.1991
890 Murakami, M., Koga, M., & Ohshima, Y. (2001). DAF-7/TGF-beta expression required for
891 the normal larval development in *C-elegans* is controlled by a presumed guanylyl
892 cyclase DAF-11. *Mechanisms of Development, 109*(1), 27-35. doi:Doi
893 10.1016/S0925-4773(01)00507-X

894 Murayama, T., Toh, Y., Ohshima, Y., & Koga, M. (2005). The dyf-3 gene encodes a novel
895 protein required for sensory cilium formation in *Caenorhabditis elegans*. *J Mol Biol,*
896 *346*(3), 677-687. doi:10.1016/j.jmb.2004.12.005
897 Myllyharju, J., & Kivirikko, K. I. (1997). Characterization of the iron- and 2-oxoglutarate-
898 binding sites of human prolyl 4-hydroxylase. *Embo Journal, 16*(6), 1173-1180.
899 doi:DOI 10.1093/emboj/16.6.1173
900 Nicholls, P., & Kim, J. K. (1982). Sulphide as an inhibitor and electron donor for the
901 cytochrome c oxidase system. *Can J Biochem, 60*(6), 613-623. doi:10.1139/o82-076
902 Niu, W., Lu, Z. J., Zhong, M., Sarov, M., Murray, J. I., Brdlik, C. M., . . . Reinke, V. (2011).
903 Diverse transcription factor binding features revealed by genome-wide ChIP-seq in
904 *C. elegans*. *Genome Research, 21*(2), 245-254. doi:10.1101/gr.114587.110
905 Ochi, R., Dhagia, V., Lakhkar, A., Patel, D., Wolin, M. S., & Gupte, S. A. (2016). Rotenone-
906 stimulated superoxide release from mitochondrial complex I acutely augments L-type
907 Ca^{2+} current in A7r5 aortic smooth muscle cells. *Am J Physiol Heart Circ Physiol,*
908 *310*(9), H1118-1128. doi:10.1152/ajpheart.00889.2015
909 Olson, K. R., & Straub, K. D. (2016). The Role of Hydrogen Sulfide in Evolution and the
910 Evolution of Hydrogen Sulfide in Metabolism and Signaling. *Physiology (Bethesda),*
911 *31*(1), 60-72. doi:10.1152/physiol.00024.2015
912 Onukwufor, J. O., Farooqi, M. A., Vodickova, A., Koren, S. A., Baldzizhar, A., Berry, B. J., .
913 . . Wojtovich, A. P. (2022). A reversible mitochondrial complex I thiol switch
914 mediates hypoxic avoidance behavior in *C. elegans*. *Nat Commun, 13*(1), 2403.
915 doi:10.1038/s41467-022-30169-y
916 Oshins, C., Michel, F., Louis, P., Richard, T. L., & Rynk, R. (2022). Chapter 3 - The
917 composting process. In R. Rynk (Ed.), *The Composting Handbook* (pp. 51-101):
918 Academic Press.
919 Patange, O., Breen, P., Arsuffi, G., & Ruvkun, G. (2025). Hydrogen sulfide mediates the
920 interaction between *C. elegans* and Actinobacteria from its natural microbial
921 environment. *Cell Reports, 44*(1), 115170. doi:10.1016/j.celrep.2024.115170

922 Patten, D. A., Germain, M., Kelly, M. A., & Slack, R. S. (2010). Reactive oxygen species:
923 stuck in the middle of neurodegeneration. *J Alzheimers Dis, 20 Suppl 2*, S357-367.
924 doi:10.3233/JAD-2010-100498
925 Persson, A., Gross, E., Laurent, P., Busch, K. E., Bretes, H., & de Bono, M. (2009). Natural
926 variation in a neural globin tunes oxygen sensing in wild *Caenorhabditis elegans*.
927 *Nature, 458*(7241), 1030-1033. doi:10.1038/nature07820
928 Pettinati, I., Brem, J., McDonough, M. A., & Schofield, C. J. (2015). Crystal structure of
929 human persulfide dioxygenase: structural basis of ethylmalonic encephalopathy. *Hum*
930 *Mol Genet, 24*(9), 2458-2469. doi:10.1093/hmg/ddv007
931 Pfenninger, M., Lerp, H., Tobler, M., Passow, C., Kelley, J. L., Funke, E., . . . Plath, M.
932 (2014). Parallel evolution of cox genes in H_2S-tolerant fish as key adaptation to a
933 toxic environment. *Nat Commun, 5*, 3873. doi:10.1038/ncomms4873
934 Philipp, T. M., Gong, W., Kohnlein, K., Ohse, V. A., Muller, F. I., Priebs, J., . . . Klotz, L. O.
935 (2022). SEMO-1, a novel methanethiol oxidase in *Caenorhabditis elegans*, is a pro-
936 aging factor conferring selective stress resistance. *Biofactors, 48*(3), 699-706.
937 doi:10.1002/biof.1836
938 Powell-Coffman, J. A. (2010). Hypoxia signaling and resistance in *C. elegans*. *Trends*
939 *Endocrinol Metab, 21*(7), 435-440. doi:10.1016/j.tem.2010.02.006
940 Qabazard, B., Li, L., Gruber, J., Peh, M. T., Ng, L. F., Kumar, S. D., . . . Moore, P. K. (2014).
941 Hydrogen sulfide is an endogenous regulator of aging in *Caenorhabditis elegans*.
942 *Antioxid Redox Signal, 20*(16), 2621-2630. doi:10.1089/ars.2013.5448
943 Rajan, M., Anderson, C. P., Rindler, P. M., Romney, S. J., Ferreira Dos Santos, M. C., Gertz,
944 J., & Leibold, E. A. (2019). NHR-14 loss of function couples intestinal iron uptake
945 with innate immunity in *C. elegans* through PQM-1 signaling. *Elife, 8*.
946 doi:10.7554/eLife.44674
947 Ramsay, R. R., & Singer, T. P. (1992). Relation of superoxide generation and lipid
948 peroxidation to the inhibition of NADH-Q oxidoreductase by rotenone, piericidin A,

949 and MPP+. *Biochem Biophys Res Commun, 189*(1), 47-52. doi:10.1016/0006-
950 291x(92)91523-s
951 Read, A. D., Bentley, R. E. T., Archer, S. L., & Dunham-Snary, K. J. (2021). Mitochondrial
952 iron-sulfur clusters: Structure, function, and an emerging role in vascular biology.
953 *Redox Biology, 47*. doi:ARTN 102164
954 10.1016/j.redox.2021.102164
955 Rodriguez-Kabana, R., Jordan, J. W., & Hollis, J. P. (1965). Nematodes: Biological Control
956 in Rice Fields: Role of Hydrogen Sulfide. *Science, 148*(3669), 524-526.
957 doi:10.1126/science.148.3669.524
958 Romanelli-Cedrez, L., Vairoletti, F., & Salinas, G. (2024). Rhodoquinone-dependent electron
959 transport chain is essential for *Caenorhabditis elegans* survival in hydrogen sulfide
960 environments. *J Biol Chem, 300*(9), 107708. doi:10.1016/j.jbc.2024.107708
961 Romney, S. J., Newman, B. S., Thacker, C., & Leibold, E. A. (2011). HIF-1 regulates iron
962 homeostasis in *Caenorhabditis elegans* by activation and inhibition of genes involved
963 in iron uptake and storage. *PLoS Genet, 7*(12), e1002394.
964 doi:10.1371/journal.pgen.1002394
965 Salvanes, A. G. V., Utne-Palm, A. C., Currie, B., & Braithwaite, V. A. (2011). Behavioural
966 and physiological adaptations of the bearded goby, a key fish species of the extreme
967 environment of the northern Benguela upwelling. *Marine Ecology Progress Series,*
968 *425*, 193-202. doi:10.3354/meps08998
969 Schiavo, G., Benfenati, F., Poulain, B., Rossetto, O., Polverino de Laureto, P., DasGupta, B.
970 R., & Montecucco, C. (1992). Tetanus and botulinum-B neurotoxins block
971 neurotransmitter release by proteolytic cleavage of synaptobrevin. *Nature, 359*(6398),
972 832-835. doi:10.1038/359832a0
973 Semenza, G. L. (2010). Defining the role of hypoxia-inducible factor 1 in cancer biology and
974 therapeutics. *Oncogene, 29*(5), 625-634. doi:10.1038/onc.2009.441

975 Starich, T. A., Herman, R. K., Kari, C. K., Yeh, W. H., Schackwitz, W. S., Schuyler, M. W., .
976 . . Riddle, D. L. (1995). Mutations affecting the chemosensory neurons of
977 *Caenorhabditis elegans*. *Genetics, 139*(1), 171-188. doi:10.1093/genetics/139.1.171
978 Sterken, M. G., Snoek, L. B., Kammenga, J. E., & Andersen, E. C. (2015). The laboratory
979 domestication of *Caenorhabditis elegans*. *Trends Genet, 31*(5), 224-231.
980 doi:10.1016/j.tig.2015.02.009
981 Swoboda, P., Adler, H. T., & Thomas, J. H. (2000). The RFX-type transcription factor DAF-
982 19 regulates sensory neuron cilium formation in *C. elegans*. *Mol Cell, 5*(3), 411-421.
983 doi:10.1016/s1097-2765(00)80436-0
984 Szabo, C., Ransy, C., Módis, K., Andriamihaja, M., Murghes, B., Coletta, C., . . . Bouillaud,
985 F. (2014). Regulation of mitochondrial bioenergetic function by hydrogen sulfide.
986 Part I. Biochemical and physiological mechanisms. *British Journal of Pharmacology,*
987 *171*(8), 2099-2122. doi:10.1111/bph.12369
988 Vora, M., Pyonteck, S. M., Popovitchenko, T., Matlack, T. L., Prashar, A., Kane, N. S., . . .
989 Rongo, C. (2022). The hypoxia response pathway promotes PEP carboxykinase and
990 gluconeogenesis in *C. elegans*. *Nature Communications, 13*(1). doi:ARTN 6168
991 10.1038/s41467-022-33849-x
992 Weir, E. K., Lopez-Barneo, J., Buckler, K. J., & Archer, S. L. (2005). Acute oxygen-sensing
993 mechanisms. *N Engl J Med, 353*(19), 2042-2055. doi:10.1056/NEJMra050002
994 Xu, X. M., & Moller, S. G. (2011). Iron-Sulfur Clusters: Biogenesis, Molecular Mechanisms,
995 and Their Functional Significance. *Antioxidants & Redox Signaling, 15*(1), 271-307.
996 doi:10.1089/ars.2010.3259
997 Yang, W., & Hekimi, S. (2010). A mitochondrial superoxide signal triggers increased
998 longevity in *Caenorhabditis elegans*. *PLoS Biol, 8*(12), e1000556.
999 doi:10.1371/journal.pbio.1000556
1000 Zhao, L., Fenk, L. A., Nilsson, L., Amin-Wetzel, N. P., Ramirez-Suarez, N. J., de Bono, M.,
1001 & Chen, C. (2022). ROS and cGMP signaling modulate persistent escape from

1002 hypoxia in *Caenorhabditis elegans*. *PLoS Biol, 20*(6), e3001684.
1003 doi:10.1371/journal.pbio.3001684
1004 Zimmer, M., Gray, J. M., Pokala, N., Chang, A. J., Karow, D. S., Marletta, M. A., . . .
1005 Bargmann, C. I. (2009). Neurons detect increases and decreases in oxygen levels
1006 using distinct guanylate cyclases. *Neuron, 61*(6), 865-879.
1007 doi:10.1016/j.neuron.2009.02.013
1008 Zorov, D. B., Juhaszova, M., & Sollott, S. J. (2014). Mitochondrial reactive oxygen species
1009 (ROS) and ROS-induced ROS release. *Physiol Rev, 94*(3), 909-950.
1010 doi:10.1152/physrev.00026.2013
1011 Zubovych, I. O., Straud, S., & Roth, M. G. (2010). Mitochondrial dysfunction confers
1012 resistance to multiple drugs in *Caenorhabditis elegans*. *Mol Biol Cell, 21*(6), 956-
1013 969. doi:10.1091/mbc.e09-08-0673
1014
1015 **Figure legends**
1016 **Figure 1. Acute locomotory responses of *C. elegans* to hydrogen sulfide**
1017 (**A**) Changes in the locomotory speed of WT animals (N2 laboratory strain) evoked by a switch
1018 from 7% O_2 to 150 ppm H_2S balanced with 7% O_2, followed by a return to 7% O_2. (**B**)
1019 Proportion of WT animals undergoing reorientation movements (omega turns) during a switch
1020 from 7% O_2 to 150 ppm H_2S balanced with 7% O_2, followed by a return to 7% O_2. (**C**) Fraction
1021 of WT animals doing backward locomotion (reversals) during a switch from 7% O_2 to 150 ppm
1022 H_2S balanced with 7% O_2, followed by a return to 7% O_2. (**D**) Locomotory speed of WT was
1023 recorded for 2 minutes at 7% O_2, followed by 148 minutes at 150 ppm H_2S balanced with 7%
1024 O_2, and then at 7% O_2. (**E**) Locomotory speed of WT animals in response to near-UV light (435
1025 nm, 0.7 mW/mm^2) exposure, before and directly after 30-minute preincubation in 150 ppm H_2S
1026 balanced with 7% O_2. Locomotory activity was recorded for 2 minutes before, during and after
1027 UV light exposure. (**F**) Locomotory speed of WT animals to different concentrations of H_2S
1028 balanced with 7% O_2. Red bars on the x-axis represent two intervals (4–5 minutes and 11–12
1029 minutes, labeled a and b, respectively) used for statistical analysis. **** = $p < 0.0001$, ** = $p <$

1030 0.01, * = $p < 0.05$, ns = not significant, Mann–Whitney U test. (**G**) Distribution of WT animals
1031 in a microfluidic device after 25 minutes of aerotaxis. The gas inputs and the five chamber
1032 sections used for scoring are indicated. (**H**) Distribution of WT animals in a gradient of H_2S
1033 (150 ppm to 0 ppm). The bins correspond to different sections of the microfluidic chamber
1034 described in (**G**). N= 4 aerotaxis assays.
1035
1036 **Figure 2. Neurosecretion from ASJ neurons contributes to H_2S avoidance**
1037 (**A–H**) Locomotory speed responses to a switch from 7% O_2 to 150 ppm H_2S balanced with 7%
1038 O_2 for animals of the indicated genotype: WT and *daf-19(m86)* (**A**); WT and *dyf-3(m185)* (**B**);
1039 WT and *dyf-7(m539)* (**C**); WT, *daf-11(m47)* and *tax-4(p678)* (**D**); WT and *tax-2(p691)* (**E**);
1040 WT, *daf-11(m47)* and transgenic *daf-11(m47)* expressing *daf-11* genomic DNA in ASJ neurons
1041 (two independent lines) (**F**); WT, *tax-4(p678)* and transgenic *tax-4(p678)* expressing *tax-4*
1042 cDNA in ASJ neurons (two independent lines) (**G**); WT and transgenic WT expressing the
1043 catalytic domain of the *tetanus* toxin (TeTx) in ASJ neurons (**H**). For the comparison of acute
1044 locomotory speed responses between strains, red bars on the x-axis represent two intervals (4–
1045 5 minutes and 11–12 minutes, labeled a and b, respectively, in panels D, F, and G) used for
1046 statistical analysis. **** = $p < 0.0001$, *** = $p < 0.001$, ** = $p < 0.01$, * = $p < 0.05$, ns = not
1047 significant, Mann–Whitney U test.
1048
1049 **Figure 3. Insulin, TGF-β, and high O_2 signaling pathways antagonizes H_2S avoidance**
1050 (**A, B**) Locomotory speed responses to a switch from 7% O_2 to 150 ppm H_2S balanced with 7%
1051 O_2 for animals of the indicated genotype: WT, *daf-2(e1370), daf-16(mgDf47)*, and *daf-2(e1370);*
1052 *daf-16(mgDf47)* double mutants (**A**); WT, *daf-7(e1372), daf-3(mgDf90),* and *daf-7(e1372);*
1053 *daf-3(mgDf90)* double mutants (**B**). For the *daf-2* assays, WT and *daf-2* mutants were
1054 maintained at 15°C. L4 animals were picked and shifted to 25°C until day-one adults, then
1055 assayed at room temperature. (**C**) Hypothetical model for the regulation of H_2S avoidance by a
1056 starvation program involving the insulin, TGF-β, and NHR-49 pathways. (**D**) Locomotory
1057 speed response to a switch from 7% O_2 to 150 ppm H_2S balanced with 7% O_2 in fed and starved

1058 WT animals. (**E, F**) Locomotory speed responses to a switch from 7% O_2 to 150 ppm H_2S
1059 balanced with 7% O_2 for animals of the indicated genotype: WT and wild isolates (CB4858 and
1060 CB4855) (**E**); WT and *npr-1(ad609)* (**F**). (**G**) Hypothetical model showing how O_2 regulates
1061 H_2S avoidance via the inhibitory RMG circuit activity, which is modulated by O_2 sensory inputs
1062 and NPR-1 signaling. (**H–L**) Locomotory speed responses to a switch from 7% O_2 to 150 ppm
1063 H_2S balanced with 7% O_2 for animals of the indicated genotype: WT, *npr-1(ad609)*, and
1064 transgenic *npr-1(ad609)* expressing *npr-1* in RMG neurons using Cre-LoxP system (Macosko
1065 et al., 2009) (**H**); WT, *npr-1(ad609), gcy-35(ok769)*, and *npr-1(ad609); gcy-35(ok769)* double
1066 mutants (**I**); WT, *npr-1(ad609), tax-4(p678)* and *npr-1(ad609); tax-4(p678)* double mutants (**J**);
1067 WT, *npr-1(ad609), qaIs2241*(genetic ablation of AQR, PQR and URX neurons) and *npr-*
1068 *1(ad609); qaIs 2241* (**K**); WT, *npr-1(ad609), npr-1(ad609); gcy-35(ok769)* double mutants and
1069 *transgenic npr-1(ad609); gcy-35(ok769)* double mutants expressing *gcy-35* cDNA under *gcy-*
1070 *37* promoter, which drives *gcy-35* expression in O_2 sensing neurons (**L**). For the comparison of
1071 acute locomotory responses between strains, red bars on the x-axis represent two intervals (4–
1072 5 minutes and 11–12 minutes, labeled a and b, respectively, in panel E) used for statistical
1073 analysis. **** = $p < 0.0001$, *** = $p < 0.001$, ** = $p < 0.01$, * = $p < 0.05$, ns = not significant,
1074 Mann–Whitney U test.
1075
1076 **Figure 4. Prolonged H_2S exposure reprograms gene expression in *C. elegans***
1077 (**A**) Venn diagram displaying the number of differentially expressed genes after 1-hour
1078 exposure to 50 ppm or 150 ppm H_2S balanced with 7% O_2 in WT animals (adjusted $p < 1e-10$).
1079 (**B**) Venn diagram displaying the number of differentially expressed genes after 1-, 2-, and 12-
1080 hour exposure to 150 ppm H_2S balanced with 7% O_2 in WT animals (adjusted $p < 1e-10$). (**C,**
1081 **D**) Significantly enriched GO categories for differentially expressed genes with adjusted $p <$
1082 1e-10 in WT animals exposed to 50 ppm (**C**) or 150 ppm (**D**) H_2S balanced with 7% O_2 for 1
1083 hour. (**E, F**) Volcano plots showing the differentially expressed genes with adjusted $p < 1e-10$
1084 in WT animals exposed to 50 ppm (**E**) or 150 ppm (**F**) H_2S balanced with 7% O_2 for 1 hour. A

1085 set of genes involved in H_2S detoxification, cysteine metabolism and stress response were
1086 highlighted in red.
1087
1088 **Figure 5. Acute response to H_2S is modulated by HIF-1 signaling**
1089 (**A**) Locomotory speed responses of WT animals to a switch from 7% O_2 to 150 ppm H_2S
1090 balanced with 7% O_2 after incubation of the animals for 0, 12, 24, or 36 hours in 1% O_2. (**B, C**)
1091 Locomotory speed responses to a switch from 7% O_2 to 150 ppm H_2S balanced with 7% O_2 for
1092 animals of the indicated genotype: WT, *egl-9(sa307)*, and *vhl-1(ok161)* (**B**); WT and transgenic
1093 animals expressing the non-degradable form of HIF-1 (P621A or P621G) under the pan-
1094 neuronal *unc-14* promoter or the endogenous *hif-1* promoter, respectively (**C**). (**D–F**)
1095 Avoidance responses of WT and *hif-1(ia4)* to a switch from 7% O_2 to 150 ppm H_2S balanced
1096 with 7% O_2, including locomotory speed (**D**), reorientation (omega-turn) (**E**), and reversal (**F**).
1097 (**G, H**) Locomotory speed responses to a switch from 7% O_2 to 150 ppm H_2S balanced with 7%
1098 O_2 for animals of the indicated genotype: WT, *egl-9(sa307), hif-1(ia4)*, and *egl-9(sa307); hif-*
1099 *1(ia4)* double mutants (**G**); WT, *vhl-1(ok161), hif-1(ia4)*, and *vhl-1(ok161); hif-1(ia4)* double
1100 mutants (**H**). (**I**) Average locomotory speed during 2 minutes of exposure to near-UV light for
1101 WT, *hif-1(ia4)*, and *egl-9(sa307)* before (Ctrl = control) and after 30 minutes of exposure to
1102 150 ppm H_2S balanced with 7% O_2. (**J–L**) Locomotory speed responses to a switch from 7%
1103 O_2 to 150 ppm H_2S balanced with 7% O_2 for animals of the indicated genotype: WT and *sqrd-*
1104 *1(tm3378)* (**J**); WT and *ethe-1(yum2895)* (**K**); WT, *cysl-1(ok762), cysl-2(ok3516)*, and *cysl-*
1105 *3(yum4)* (**L**). For the comparison of acute locomotory responses between strains, red bars on
1106 the x-axis represent two intervals (4–5 minutes and 11–12 minutes, labeled a and b, respectively,
1107 in panels A, B, C, and L) used for statistical analysis. *** = $p < 0.001$, ** = $p < 0.01$, * = $p <$
1108 0.05, ns = not significant, Mann–Whitney U test.
1109
1110 **Figure 6. Labile iron pool sustains the locomotory activity in H_2S**
1111 (**A, B**) Volcano plots showing the relative expression of the genes involved in the regulation of
1112 iron homeostasis in WT animals after 2-hour exposure in 50 ppm (**A**) or 150 ppm (**B**) H_2S

1113 balanced with 7% O_2. (**C–G**) Locomotory speed responses to a switch from 7% O_2 to 150 ppm
1114 H_2S balanced with 7% O_2 for animals of indicated genotypes or treatments: WT and animals
1115 overexpressing *ftn-1* genomic DNA under its own promoter (#1 and #2 indicate two
1116 independent lines) (**C**); WT, *smf-3(ok1305)*, and *ftn-1(ok3625)* (**D**); WT, and WT pretreated
1117 with 100 μM 2,2′-Bipyridyl (BP) or with 5 mg/ml ferric ammonium citrate (FAC) in the
1118 presence of food for 16 hours (**E**); WT, *hif-1(ia4)*, and *hif-1(ia4)* mutants pretreated with 5
1119 mg/ml ferric ammonium citrate (FAC) for 16 hours (**F**); WT, *hif-1(ia4), ftn-1(ok3625)*, and *hif-*
1120 *1(ia4); ftn-1(ok3625)* double mutants (**G**). (**H**) Hypothetical model of the interactions between
1121 labile iron pool and HIF-1 signaling. For the comparison of acute locomotory speed responses
1122 between strains or conditions, red bars on the x-axis represent two intervals (4–5 minutes and
1123 11–12 minutes, labeled a and b, respectively, in panels C, D, and E) used for statistical analysis.
1124 **** = $p < 0.0001$, *** = $p < 0.001$, ** = $p < 0.01$, * = $p < 0.05$, ns = not significant, Mann–
1125 Whitney U test.
1126
1127 **Figure 7. Mitochondrial function is required for acute response to H_2S**
1128 (**A–D**) Locomotory speed responses to a switch from 7% O_2 to 150 ppm H_2S balanced with 7%
1129 O_2 for animals of the indicated genotype: WT and *gas-1(fc21)* (**A**); WT and *clk-1(qm30)* (**B**);
1130 WT and *mev-1(kn1)* (**C**); WT and *isp-1(qm150)* (**D**). (**E**) Locomotory speed responses to a
1131 switch from 7% O_2 to 150 ppm H_2S balanced with 7% O_2 for WT animals pretreated with 10
1132 μM rotenone for 0 minute, 10 minutes, 30 minutes, 60 minutes or 120 minutes. For the
1133 comparison of acute locomotory speed responses between strains or conditions, red bars on the
1134 x-axis represent two intervals (4–5 minutes and 11–12 minutes) used for statistical analysis.
1135 *** = $p < 0.001$, ** = $p < 0.01$, * = $p < 0.05$, ns = not significant, Mann–Whitney U test. (**F–**
1136 **G**) Locomotory speed responses to a switch from 7% O_2 to 150 ppm H_2S balanced with 7% O_2
1137 for animals of the indicated genotype: WT, *sod-1(tm776)*, *sod-2(ok1030)*, and *sod-3(tm760)*
1138 (**F**); WT, *sod-4(gk101)*, *sod-5(tm1146)*, and *sod-1(tm783); sod-2(ok1030); sod-3(tm760); sod-*
1139 *4(gk101); sod-5 (tm1146)* (**G**). For the comparison of acute locomotory speed responses
1140 between strains or conditions, red bars on the x-axis represent the time interval (6–10 minutes)

1141 used for statistical analysis. *** = $p < 0.001$, ** = $p < 0.01$, * = $p < 0.05$, ns = not significant,
1142 Mann–Whitney U test. (**H**) Hypothetical model of the role of mitochondria in response to toxic
1143 levels of H_2S. In this model, mitochondria play a dual role in H_2S-evoked avoidance behavior.
1144 A transient burst of mitochondrial ROS triggered by high H_2S levels initiates locomotory
1145 avoidance, whereas sustained ROS elevation activates stress-responsive pathways, including
1146 HIF-1, NRF2/SKN-1, and DAF-16/FOXO, promoting adaptation to prolonged H_2S exposure.
1147

1148 **Figure supplement legends**

1149 **Figure 2—figure supplement 1. Acute avoidance response to H_2S is regulated by cGMP**
1150 **signaling**

1151 (**A–H**) Fraction of animals undergoing reorientation movements (omega turns, left) or
1152 backward locomotion (reversals, right) during a switch from 7% O_2 to 150 ppm H_2S balanced
1153 with 7% O_2 for animals of the indicated genotype: WT and *daf-19(m86)* (**A, B**); WT and *dyf-*
1154 *3(m185)* (**C, D**); WT and *dyf-7(m539)* (**E, F**); WT, *daf-11(m47)*, and *tax-4(p678)* (**G, H**).
1155

1156 **Figure 2—figure supplement 2. Acute response to H_2S is regulated by *daf-11* signaling in**
1157 **ASJ neurons**

1158 (**A**) The detailed expression pattern of each promoter used to express *daf-11* genomic DNA.
1159 Promoters shown in green rescued the *daf-11(m47)* mutant phenotype. (**B–D**) Locomotory
1160 speed responses to a switch from 7% O_2 to 150 ppm H_2S balanced with 7% O_2 for animals of
1161 the indicated genotype: WT, *daf-11(m47)*, and transgenic *daf-11* mutants expressing *daf-11*
1162 genomic DNA in different subsets of neurons. Red bars on the x-axis represent two intervals
1163 (4–5 minutes and 11–12 minutes, labeled a and b, respectively) used for statistical analysis. *
1164 = $p < 0.05$, ns = not significant, Mann–Whitney U test. (**E**) Calcium transients evoked in ASJ
1165 neurons of WT animals in response to a switch from 7% O_2 to 150 ppm H_2S balanced with 7%
1166 O_2 for animals (N=42). The slow decline in GCaMP6s fluorescence is due to photobleaching.
1167 (**F**) Calcium transients evoked in ASJ neurons of WT animals in response to a switch from 7%
1168 O_2 to 3% CO_2 balanced with 7% O_2 for animals (N=16).

1169

1170 **Figure 3—figure supplement 1. Insulin, TGF-β, and O_2 signaling modulate locomotory**
1171 **response to H_2S**

1172 (**A–C**) Locomotory speed responses to a switch from 7% O_2 to 150 ppm H_2S balanced with 7%
1173 O_2 for animals of the indicated genotype: WT and *nhr-49(nr2041)* (**A**); WT and *tax-6(ok2065)*
1174 (**B**); WT and *cnb-1(ok276)* (**C**). (**D–F**) Locomotory responses to a switch from 7% O_2 to 150
1175 ppm H_2S balanced with 7% O_2 for WT and *daf-2(e1370)*, including locomotory speed (**D**),
1176 reorientation (omega turns) (**E**), and reversal (**F**). WT and *daf-2* mutants were maintained at
1177 15°C. L4 animals were picked and shifted to 25°C until day-one adults, then assayed at room
1178 temperature. (**G–I**) Locomotory responses to a switch from 7% O_2 to 150 ppm H_2S balanced
1179 with 7% O_2 for WT and *gcy-9(tm7632)*, including locomotory speed (**G**), reorientation (omega
1180 turns) (**H**), and reversal (**I**). (**J**) Locomotory speed responses to a switch from 7% O_2 to 150
1181 ppm H_2S balanced with 7% O_2 for WT animals and wild isolate CB4856. (**K**) Optogenetic
1182 stimulation of RMG neurons using channelrhodopsin-2 (ChR2). ChR2 was expressed in RMG
1183 neurons using the Cre-LoxP system (Macosko et al., 2009). Blue light was delivered throughout
1184 the assay. Locomotory speed responses to a switch from 7% O_2 to 150 ppm H_2S balanced with
1185 7% O_2 were recorded for day-one adults grown for 16 hours in the presence or absence of ATR.
1186 (**L**) Locomotory speed responses to a switch from 7% O_2 to 150 ppm H_2S balanced with 7%
1187 O_2, following activation of O_2 sensing neurons by expressing a gain-of-function allele of *pkc-*
1188 1 in O_2 sensory neurons under *gcy-37* promoter. For the comparison of acute locomotory speed
1189 responses between strains or conditions, red bars on the x-axis represent two intervals (4–5
1190 minutes and 11–12 minutes, indicated with red bars on the x-axis) for statistical analysis. ****
1191 = $p < 0.0001$, *** = $p < 0.001$, ** = $p < 0.01$, ns = not significant, Mann–Whitney U test.

1192

1193 **Figure 4—figure supplement 1. Transcriptome reprogramming induced by H_2S exposure**

1194 (**A**) Venn diagram displaying the number of differentially expressed genes with adjusted *p*
1195 value <1e-10 in WT animals exposed to 50 ppm H_2S balanced with 7% O_2 for 1, 2, or 12 hours.
1196 (**B, C**) Significantly enriched GO categories for differentially expressed genes with adjusted *p*

1197 value <1e-10 in WT animals exposed to 50 ppm (**B**) or 150 ppm (**C**) H_2S balanced with 7% O_2
1198 for 2 hours. (**D, E**) Volcano plots showing the differentially expressed genes with adjusted *p*
1199 value <1e-10 in WT animals exposed to 50 ppm (**D**) or 150 ppm (**E**) H_2S balanced with 7% O_2
1200 for 2 hours. A set of genes involved in H_2S detoxification, cysteine metabolism and stress
1201 response are highlighted in red. (**F, G**) The number of HIF-1(**F**) and SKN-1(**G**) target genes
1202 induced by 50 ppm or 150 ppm H_2S exposure for 1 hour, 2 hours or 12 hours in WT animals,
1203 with adjusted *p* value < 1e-30. (**H–J**) Venn diagrams displaying the number of differentially
1204 expressed genes (adjusted *p* value <1e-10) in WT animals under the indicated conditions:
1205 animals exposed to 50 ppm or 150 ppm H_2S for 1hour (**H**); 2 hours (**I**); and 12 hours (**J**). (**K,**
1206 **L**) Volcano plots showing the differentially expressed genes (adjusted *p* value <1e-10) in WT
1207 animals that were exposed to either 50 ppm (**K**) or 150 ppm (**L**) H_2S balanced with 7% O_2 for
1208 12 hours. A set of genes involved in H_2S detoxification, cysteine metabolism and stress
1209 response are highlighted in red.
1210
1211 **Figure 5—figure supplement 1. Acute response to H_2S is modulated by HIF-1 signaling**
1212 (**A, B**) Fraction of WT and *egl-9(sa307)* animals undergoing reorientation movements (omega
1213 turns) (**A**) or backward locomotion (reversals) (**B**) during a switch from 7% O_2 to 150 ppm H_2S
1214 balanced with 7% O_2. (**C, D**) Locomotory speed responses to a switch from 7% O_2 to 1% O_2
1215 for WT and *egl-9(sa307)* (**C**); WT, *hif-1(ia4)*, and *semo-1(yum2889)* (**D**). (**E**) HIF-1 signaling
1216 regulates the H_2S mitochondrial detoxification pathway. The detoxification enzyme SQRD-1
1217 (sulfide:quinone oxidoreductase) oxidizes H_2S, donating electrons to ubiquinone (uq), and
1218 rhodoquinone (rq) of the mitochondrial electron transport chain (ETC). ETHE-1 (persulfide
1219 dioxygenase) oxidizes sulfur compounds to sulfite. (**F–I**) Fraction of animals undergoing
1220 reorientation movements (omega turns, F and H) or backward locomotion (reversals, G and I)
1221 during a switch from 7% O_2 to 150 ppm H_2S balanced with 7% O_2 for the indicated genotypes:
1222 WT and *sqrd-1(tm3378)* (**F, G**)*;* and WT and *ethe-1(yum2895)* (**H, I**). (**J**) Locomotory speed
1223 responses to a switch from 7% O_2 to 1% O_2 for WT, *sqrd-1(tm3378)*, and *ethe-1(yum2895)*. (**K,**
1224 **L**) Fraction of WT, *cysl-1(ok762), cysl-2(ok3516)*, and *cysl-3(yum4)* animals undergoing

1225 reorientation movements (omega turns, K) or backward locomotion (reversals, L) during a
1226 switch from 7% O_2 to 150 ppm H_2S balanced with 7% O_2. (**M**) Locomotory speed responses to
1227 a switch from 7% O_2 to 1% O_2 for WT, *cysl-1(ok762), cysl-2(ok3516)*, and *cysl-3(yum4)*
1228 animals. (**N**) Locomotory speed responses to a switch from 7% O_2 to 150 ppm H_2S balanced
1229 with 7% O_2 for WT and *semo-1(yum2889)*. (**O, P**) Fraction of animals undergoing reorientation
1230 (omega turns, **O**) or backward locomotion (reversals, **P**) in response to a switch from 7% O_2 to
1231 150 ppm H_2S balanced with 7% O_2. Comparisons of acute locomotory responses between
1232 strains were performed using two intervals (4–5 minutes and 11–12 minutes, indicated with red
1233 bars on the x-axis) for statistical analysis. *** = $p < 0.001$, ns = not significant, Mann–Whitney
1234 U test.
1235
1236 **Figure 6—figure supplement 1. Labile iron pool sustains the locomotory activity in H_2S**
1237 (**A–D**) Volcano plots showing the relative expression of the genes involved in the regulation of
1238 iron homeostasis (*ftn-1*, *ftn-2*, and *smf-3*) in WT animals under the following conditions: 1-hour
1239 exposure in 50 ppm H_2S balanced with 7% O_2 (**A**); 1-hour exposure in 150 ppm H_2S balanced
1240 with 7% O_2 (**B**); 12-hour exposure in 50 ppm H_2S balanced with 7% O_2 (**C**); and 12-hour
1241 exposure in 150 ppm H_2S balanced with 7% O_2 (**D**). (**E, F**) Locomotory speed responses to a
1242 switch from 7% O_2 to 1% O_2 for animals of the indicated genotype or treatment: WT, and two
1243 independent transgenic lines overexpressing *ftn-1* genomic DNA under its own promoter (#1
1244 and #2) (**E**); WT animals, WT animals treated with 100 μM 2,2′-Bipyridyl (BP), and WT
1245 animals treated with 5 mg/ml ferric ammonium citrate (FAC) for 16 hours (**F**). Red bar on the
1246 x-axis represents one-minute time interval (3–4 minutes) used for statistical analysis. * = $p <$
1247 0.05, ns = not significant, Mann–Whitney U test. (**G, H**) Fraction of animals undergoing
1248 reorientation movements (omega turns) (**G**) or backward locomotion (reversals) (**H**) during a
1249 switch from 7% O_2 to 150 ppm H_2S balanced with 7% O_2 for animals of the indicated genotypes
1250 WT, *smf-3(ok1305)*, and *ftn-1(ok3625)*. (**I, J**) Fraction of animals undergoing reorientation
1251 movements (omega turns) (**I**) or backward locomotion (reversals) (**J**) during a switch from 7%
1252 O_2 to 150 ppm H_2S balanced with 7% O_2 for WT animals, WT animals pretreated with either

1253 100 μM 2,2′-Bipyridyl (BP) or with 5 mg/ml ferric ammonium citrate (FAC) in the presence of
1254 food for 16 hours.
1255
1256 **Figure 7—figure supplement 1. Mitochondrial function is required for acute response to**
1257 **H_2S**
1258 (**A–D**) Fraction of animals undergoing reorientation movements (omega turns) or backward
1259 locomotion (reversals) during a switch from 7% O_2 to 150 ppm H_2S balanced with 7% O_2 for
1260 the indicated genotype or treatment: WT and *clk-1(qm30)* (**A, B**); WT and *mev-1(kn1)* (**C, D**).
1261 (**E**) Locomotory speed responses to a switch from 7% O_2 to 1% O_2 for WT, *sod-2(ok1030);* and
1262 *sod-3(tm760)*. (**F, G**) Fraction of animals undergoing reorientation movements (omega turns,
1263 **F**) or backward locomotion (reversals, **G**) during a switch from 7% O_2 to 150 ppm H_2S balanced
1264 with 7% O_2 for WT and *sod-1(tm783); sod-2(ok1030); sod-3(tm760); sod-4(gk101); sod-5*
1265 *(tm1146*). (**H**) Locomotory response to acute near UV exposure for WT and *sod-1(tm783); sod-*
1266 *2(ok1030); sod-3(tm760); sod-4(gk101); sod-5 (tm1146*) before and after 30 minutes of
1267 exposure to 150ppm H_2S.
1268
1269 **Figure 1—Video 1. The locomotory response of WT animals to H_2S**
1270 An 8x accelerated video clip (original length: 16 minutes) showing WT (N2) animals exposed
1271 to 7% O_2 for 2 minutes, followed by 11 minutes in 150 ppm H_2S, and then returned to 7% O_2.
1272 The H_2S exposure segment is highlighted and begins at the 15-second mark, corresponding to
1273 2 minutes in the original recording.

Figure 1

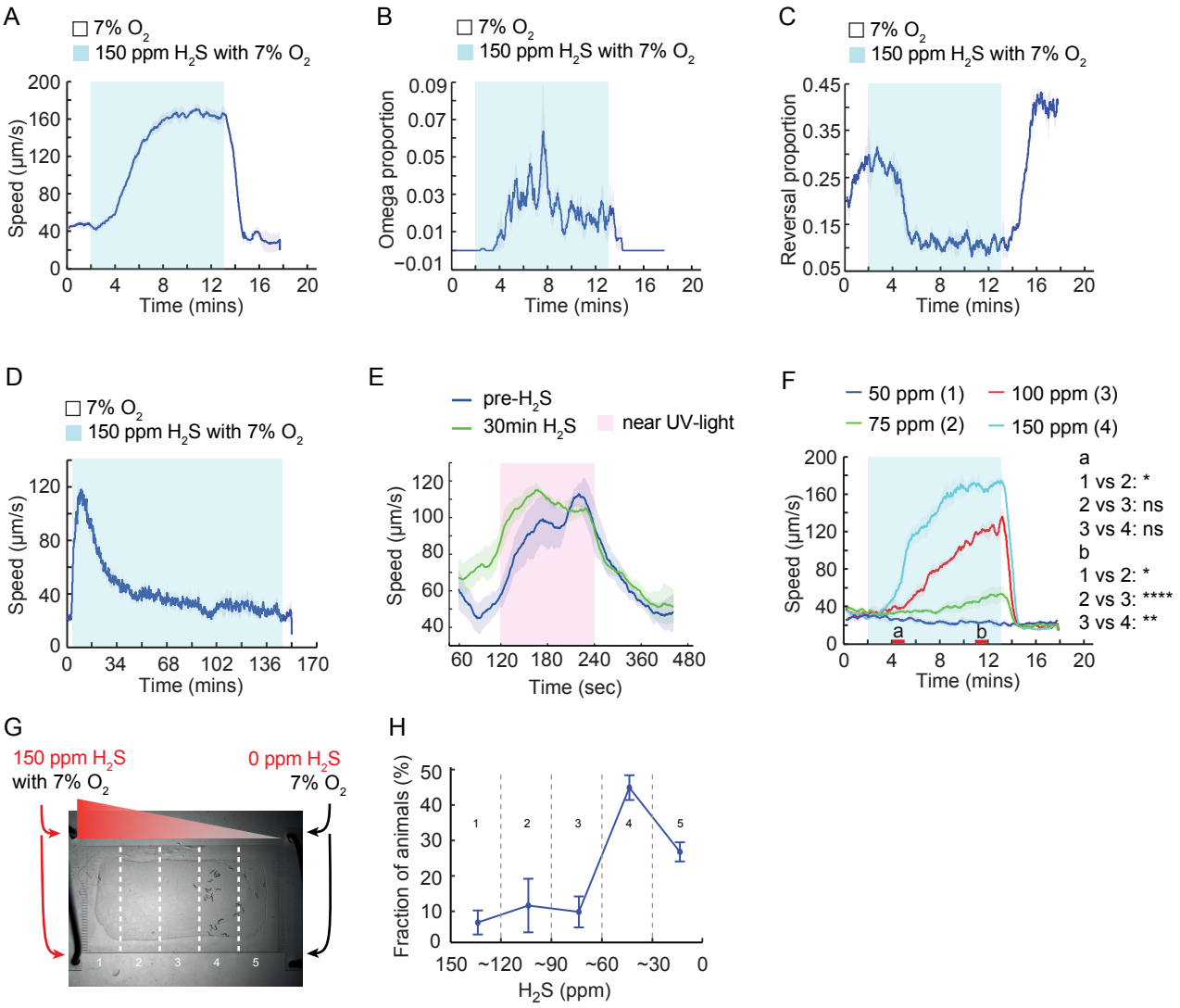
A
7% O2
150 ppm H2S with 7% O2
Speed (µm/s)
Time (mins)
B
7% O2
150 ppm H2S with 7% O2
Omega proportion
Time (mins)
C
7% O2
150 ppm H2S with 7% O2
Reversal proportion
Time (mins)
D
7% O2
150 ppm H2S with 7% O2
Speed (µm/s)
Time (mins)
E
pre-H2S
30min H2S
near UV-light
Speed (µm/s)
Time (sec)
F
50 ppm (1)
75 ppm (2)
100 ppm (3)
150 ppm (4)
Speed (µm/s)
Time (mins)
a
1 vs 2: *
2 vs 3: ns
3 vs 4: ns
b
1 vs 2: *
2 vs 3: ****
3 vs 4: **
G
150 ppm H2S
with 7% O2
0 ppm H2S
7% O2
H
Fraction of animals (%)
H2S (ppm)

Figure 2

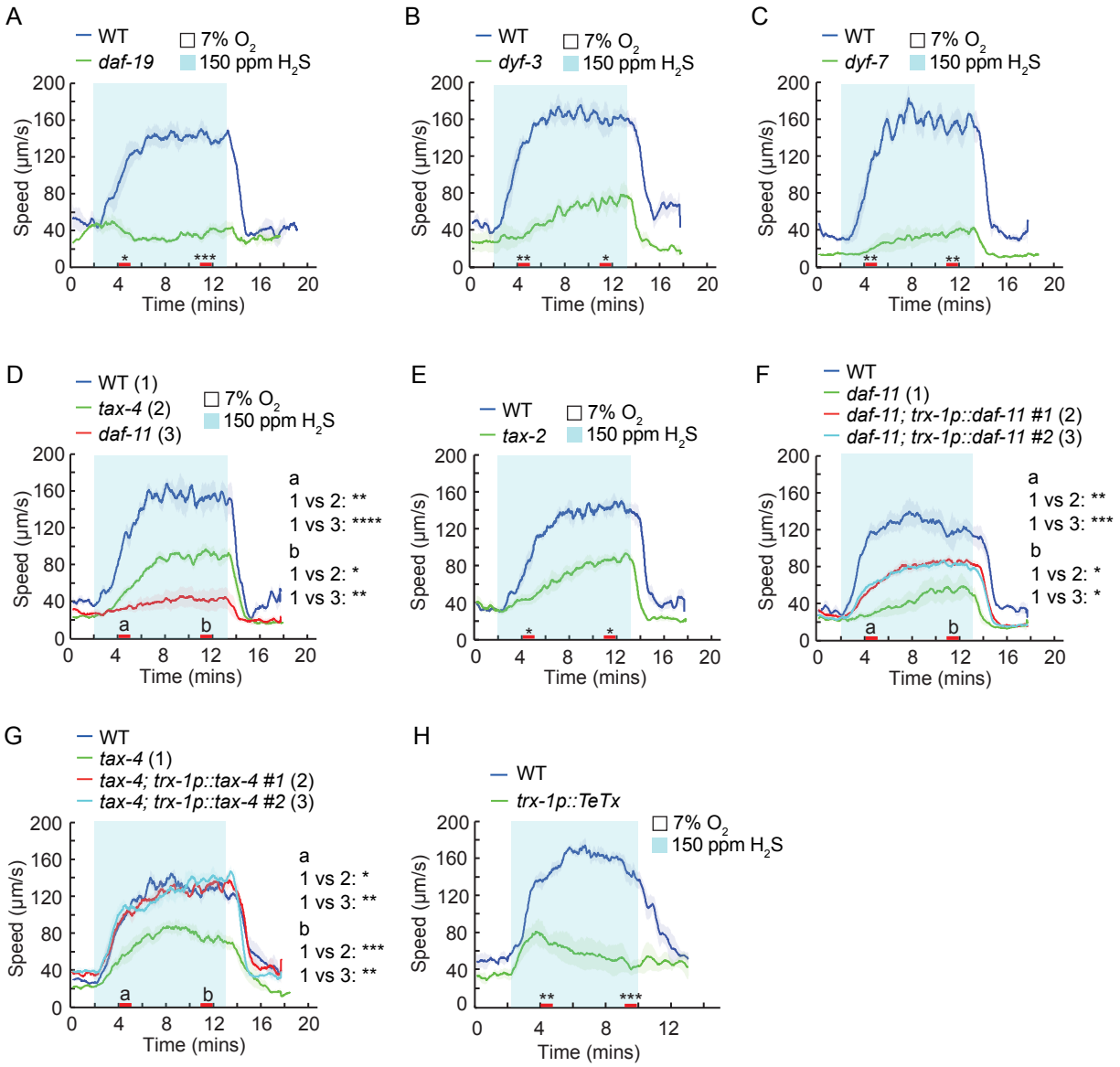
A
WT
daf-19
7% O2
150 ppm H2S
Speed (µm/s)
Time (mins)
B
WT
dyf-3
7% O2
150 ppm H2S
C
WT
dyf-7
7% O2
150 ppm H2S
D
WT (1)
tax-4 (2)
daf-11 (3)
7% O2
150 ppm H2S
a
1 vs 2: **
1 vs 3: ****
b
1 vs 2: *
1 vs 3: **
E
WT
tax-2
7% O2
150 ppm H2S
F
WT
daf-11 (1)
daf-11; trx-1p::daf-11 #1 (2)
daf-11; trx-1p::daf-11 #2 (3)
a
1 vs 2: **
1 vs 3: ***
b
1 vs 2: *
1 vs 3: *
G
WT
tax-4 (1)
tax-4; trx-1p::tax-4 #1 (2)
tax-4; trx-1p::tax-4 #2 (3)
a
1 vs 2: *
1 vs 3: **
b
1 vs 2: ***
1 vs 3: **
H
WT
trx-1p::TeTx
7% O2
150 ppm H2S

Figure 3

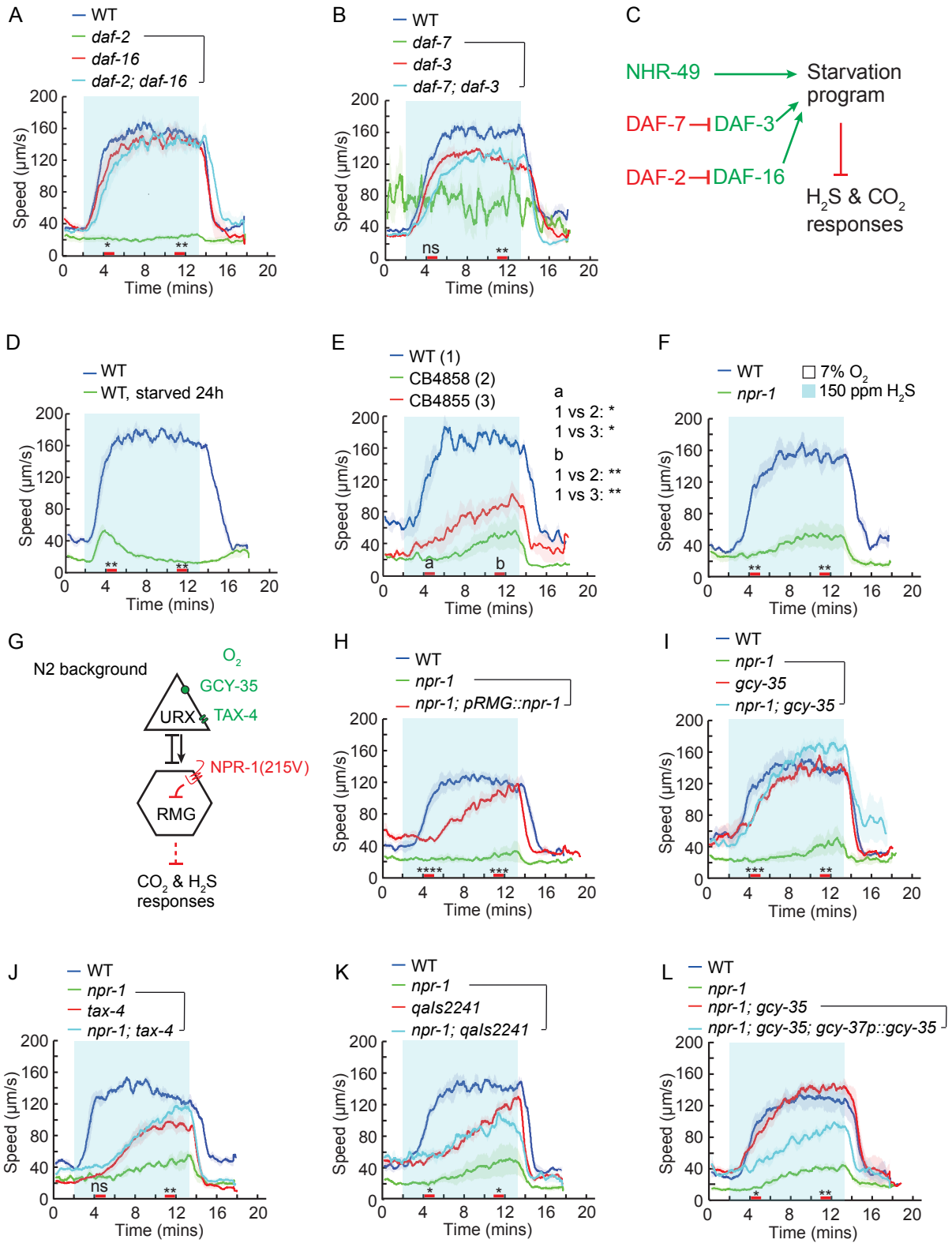
A
WT
daf-2
daf-16
daf-2; daf-16
Speed (µm/s)
Time (mins)
B
WT
daf-7
daf-3
daf-7; daf-3
ns
C
NHR-49
Starvation program
DAF-7
DAF-3
DAF-2
DAF-16
H2S & CO2 responses
D
WT
WT, starved 24h
E
WT (1)
CB4858 (2)
CB4855 (3)
a
1 vs 2: *
1 vs 3: *
b
1 vs 2: **
1 vs 3: **
F
WT
npr-1
7% O2
150 ppm H2S
G
N2 background
O2
GCY-35
TAX-4
URX
NPR-1(215V)
RMG
CO2 & H2S responses
H
WT
npr-1
npr-1; pRMG::npr-1
I
WT
npr-1
gcy-35
npr-1; gcy-35
J
WT
npr-1
tax-4
npr-1; tax-4
K
WT
npr-1
qaIs2241
npr-1; qaIs2241
L
WT
npr-1
npr-1; gcy-35
npr-1; gcy-35; gcy-37p::gcy-35

Figure 4

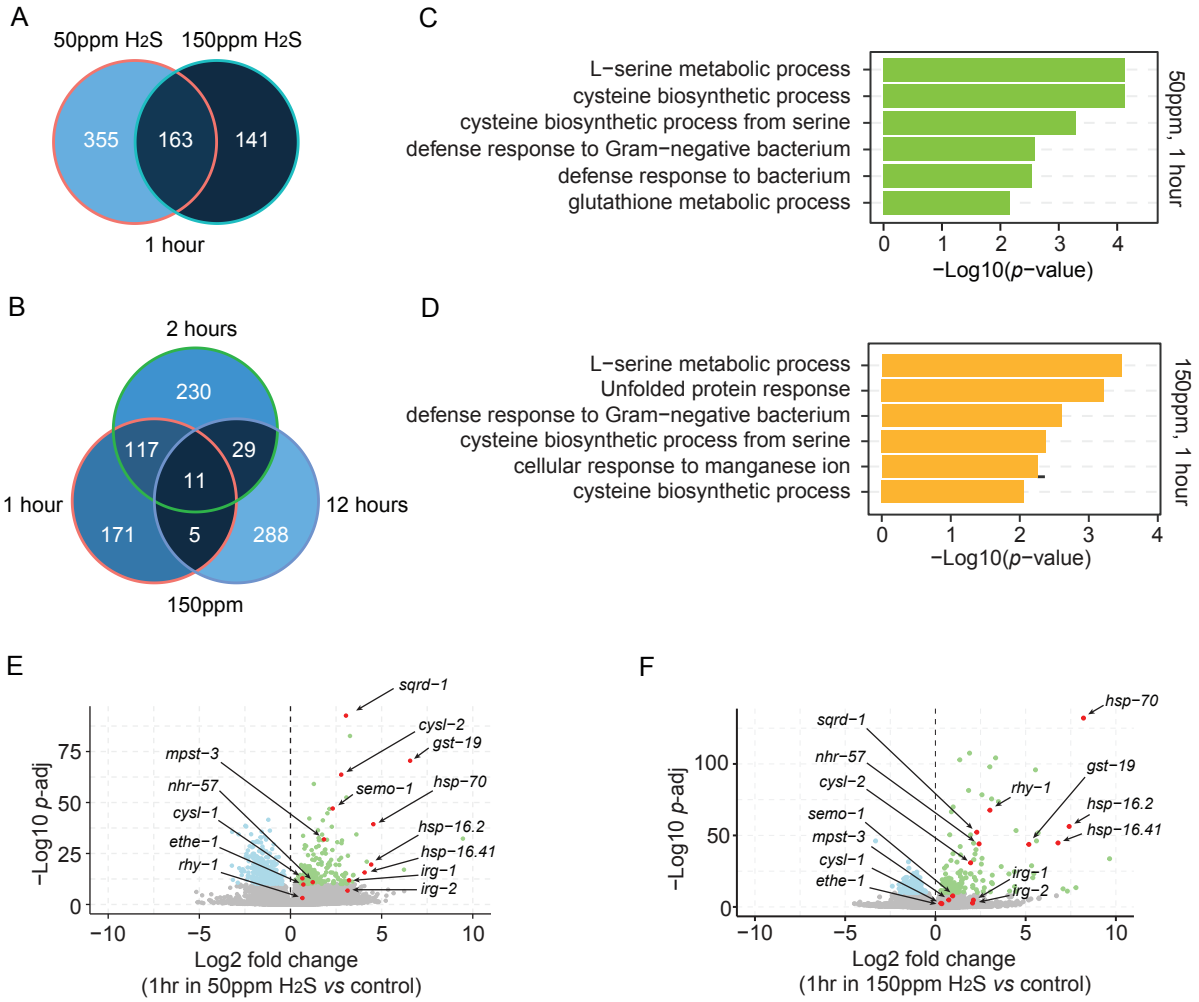
A
50ppm H2S
150ppm H2S
355
163
141
1 hour
B
2 hours
230
117
29
11
1 hour
12 hours
171
5
288
150ppm
C
L−serine metabolic process
cysteine biosynthetic process
cysteine biosynthetic process from serine
defense response to Gram−negative bacterium
defense response to bacterium
glutathione metabolic process
50ppm, 1 hour
−Log10(p−value)
D
L−serine metabolic process
Unfolded protein response
defense response to Gram−negative bacterium
cysteine biosynthetic process from serine
cellular response to manganese ion
cysteine biosynthetic process
150ppm, 1 hour
−Log10(p−value)
E
sqrd−1
cysl−2
gst−19
mpst−3
nhr−57
semo−1
hsp−70
cysl−1
hsp−16.2
ethe−1
hsp−16.41
rhy−1
irg−1
irg−2
−Log10 p-adj
Log2 fold change
(1hr in 50ppm H2S vs control)
F
hsp−70
sqrd−1
nhr−57
gst−19
cysl−2
rhy−1
semo−1
hsp−16.2
mpst−3
hsp−16.41
cysl−1
ethe−1
irg−1
irg−2
−Log10 p-adj
Log2 fold change
(1hr in 150ppm H2S vs control)

Figure 5

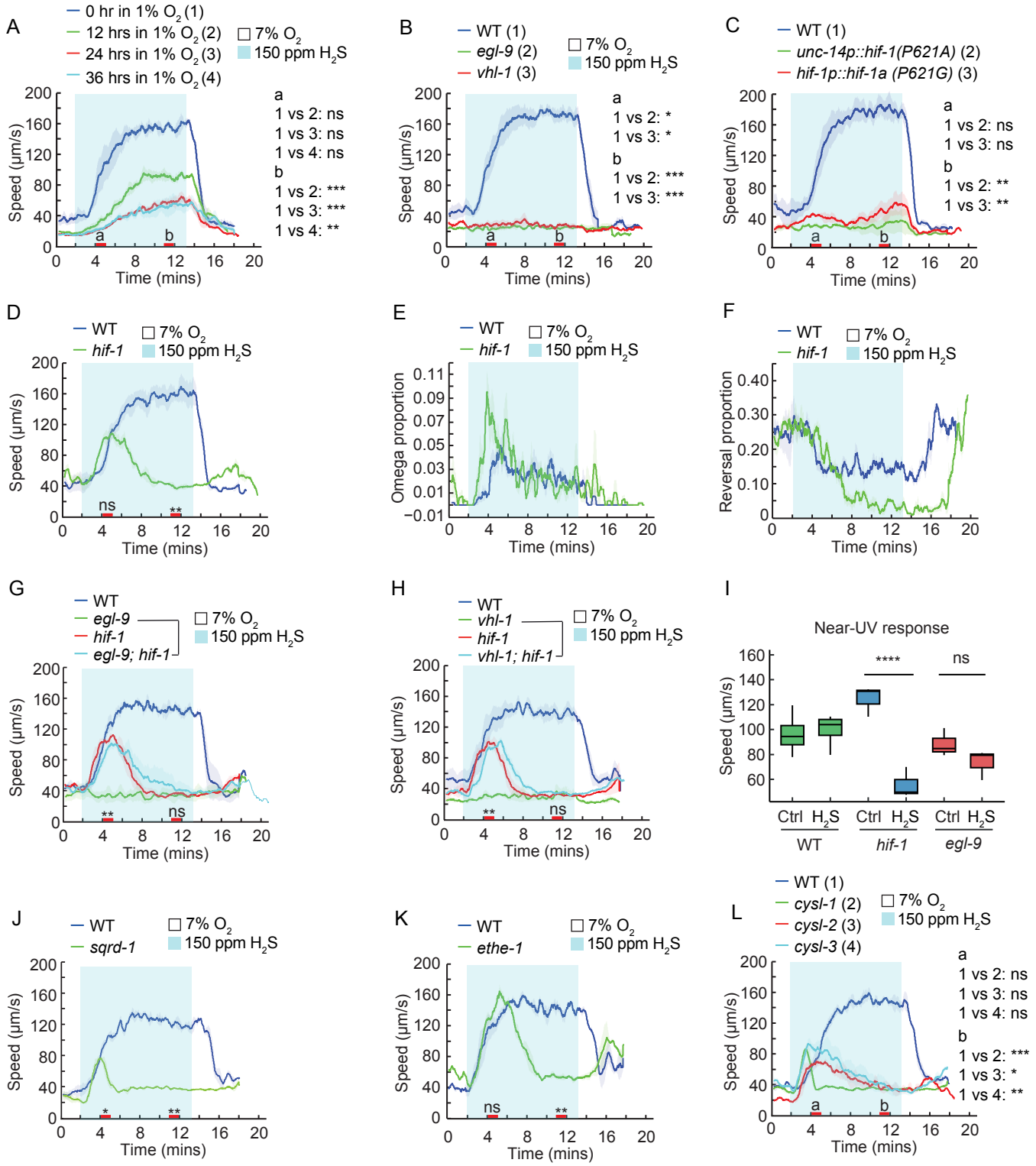
A
0 hr in 1% O2 (1)
12 hrs in 1% O2 (2)
24 hrs in 1% O2 (3)
36 hrs in 1% O2 (4)
7% O2
150 ppm H2S
a
1 vs 2: ns
1 vs 3: ns
1 vs 4: ns
b
1 vs 2: ***
1 vs 3: ***
1 vs 4: **
Speed (µm/s)
Time (mins)
B
WT (1)
egl-9 (2)
vhl-1 (3)
7% O2
150 ppm H2S
a
1 vs 2: *
1 vs 3: *
b
1 vs 2: ***
1 vs 3: ***
C
WT (1)
unc-14p::hif-1(P621A) (2)
hif-1p::hif-1a (P621G) (3)
a
1 vs 2: ns
1 vs 3: ns
b
1 vs 2: **
1 vs 3: **
D
WT
hif-1
7% O2
150 ppm H2S
ns
**
E
Omega proportion
F
Reversal proportion
G
WT
egl-9
hif-1
egl-9; hif-1
H
vhl-1
vhl-1; hif-1
I
Near-UV response
****
ns
Ctrl
H2S
WT
hif-1
egl-9
J
sqrd-1
*
K
ethe-1
L
cysl-1 (2)
cysl-2 (3)
cysl-3 (4)

Figure 6

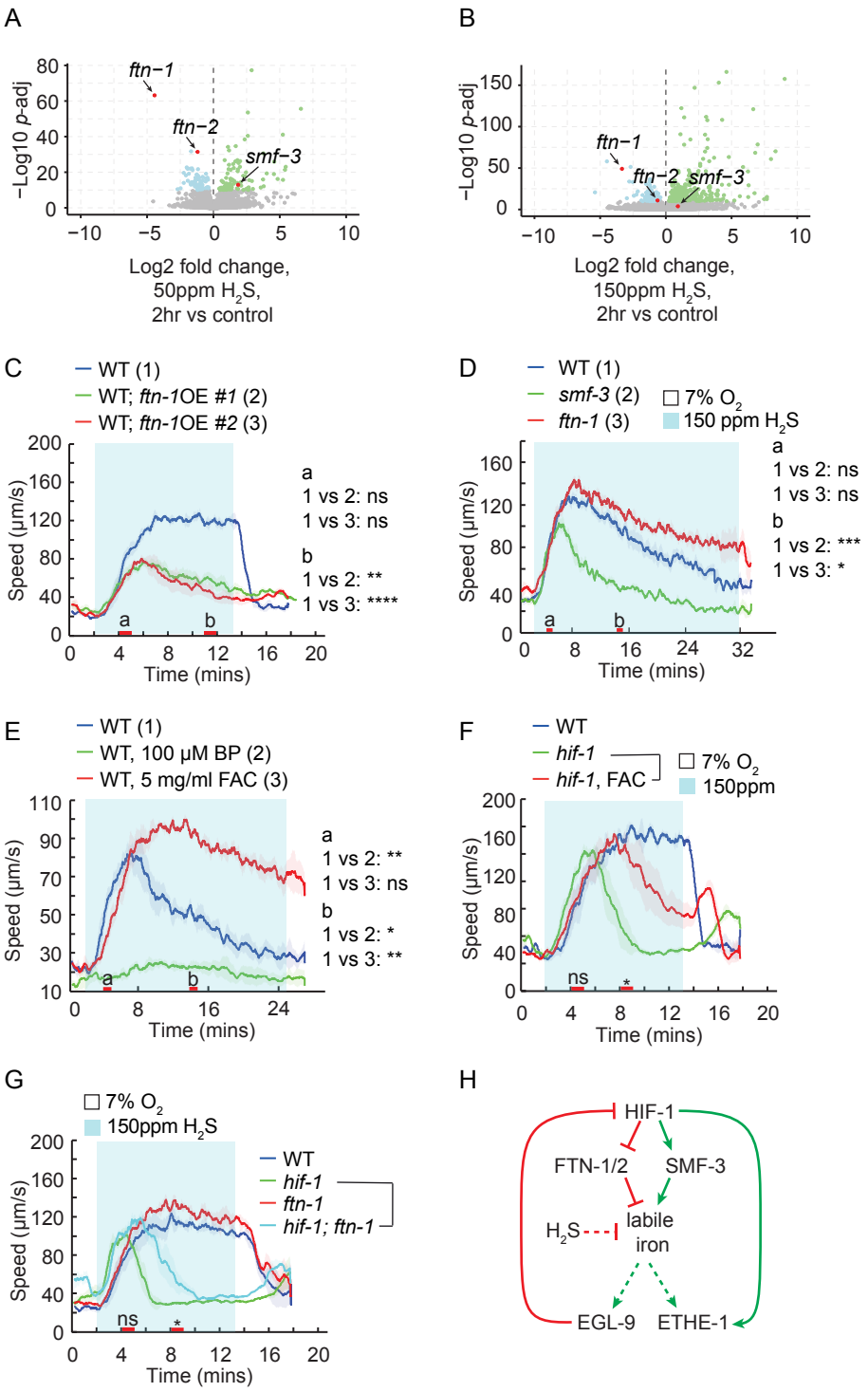
A
−Log10 p-adj
ftn−1
ftn−2
smf−3
Log2 fold change,
50ppm H2S,
2hr vs control
B
−Log10 p-adj
ftn−1
ftn−2
smf−3
Log2 fold change,
150ppm H2S,
2hr vs control
C
WT (1)
WT; ftn-1OE #1 (2)
WT; ftn-1OE #2 (3)
Speed (µm/s)
Time (mins)
a
1 vs 2: ns
1 vs 3: ns
b
1 vs 2: **
1 vs 3: ****
D
WT (1)
smf-3 (2)
ftn-1 (3)
7% O2
150 ppm H2S
Speed (µm/s)
Time (mins)
a
1 vs 2: ns
1 vs 3: ns
b
1 vs 2: ***
1 vs 3: *
E
WT (1)
WT, 100 µM BP (2)
WT, 5 mg/ml FAC (3)
Speed (µm/s)
Time (mins)
a
1 vs 2: **
1 vs 3: ns
b
1 vs 2: *
1 vs 3: **
F
WT
hif-1
hif-1, FAC
7% O2
150ppm
Speed (µm/s)
Time (mins)
ns
*
G
7% O2
150ppm H2S
WT
hif-1
ftn-1
hif-1; ftn-1
Speed (µm/s)
Time (mins)
ns
*
H
HIF-1
FTN-1/2
SMF-3
H2S
labile
iron
EGL-9
ETHE-1

Figure 7

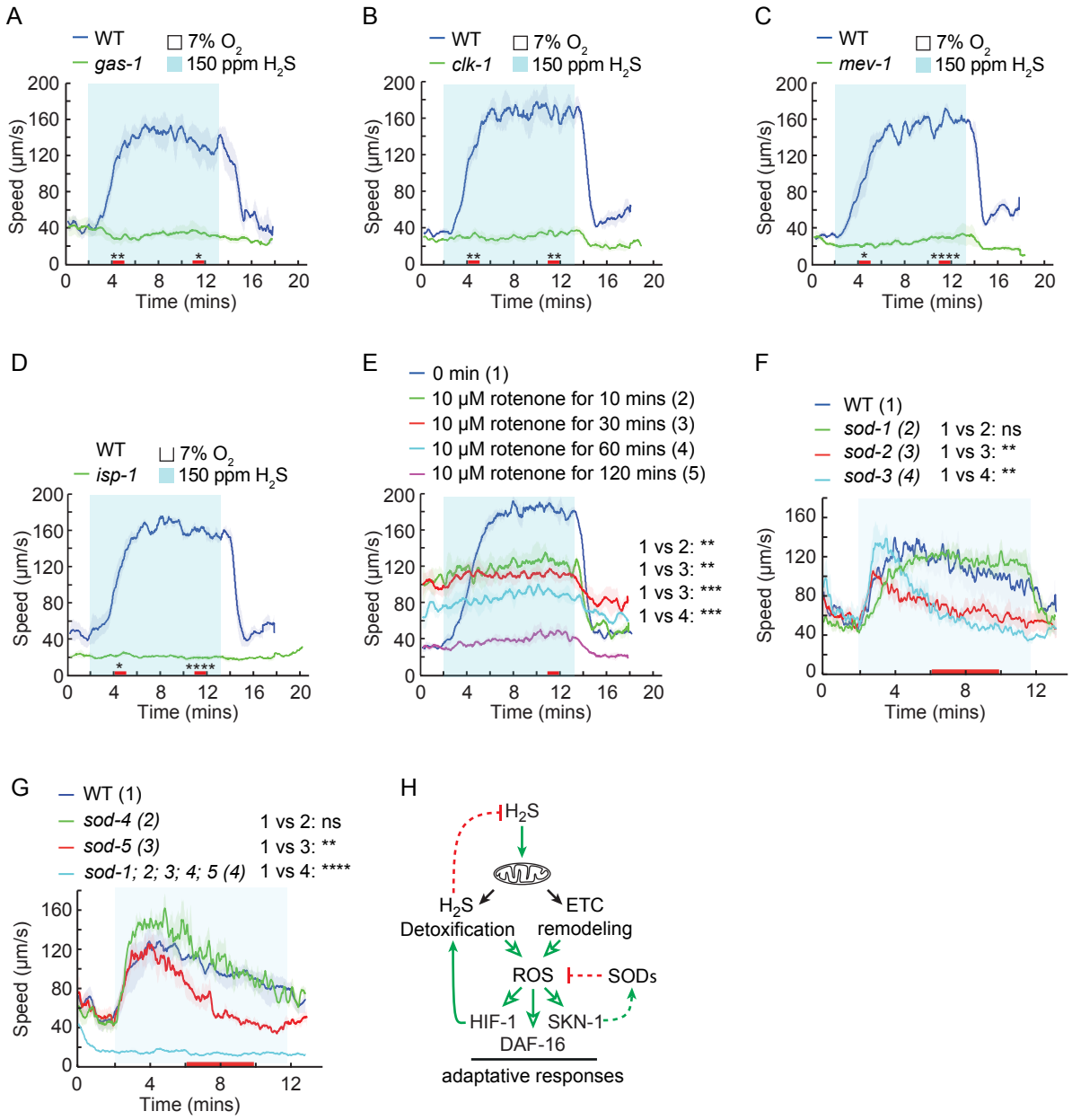
A
WT
gas-1
7% O2
150 ppm H2S
Speed (μm/s)
Time (mins)
B
WT
clk-1
7% O2
150 ppm H2S
C
WT
mev-1
7% O2
150 ppm H2S
D
WT
isp-1
7% O2
150 ppm H2S
E
0 min (1)
10 μM rotenone for 10 mins (2)
10 μM rotenone for 30 mins (3)
10 μM rotenone for 60 mins (4)
10 μM rotenone for 120 mins (5)
1 vs 2: **
1 vs 3: **
1 vs 3: ***
1 vs 4: ***
F
WT (1)
sod-1 (2) 1 vs 2: ns
sod-2 (3) 1 vs 3: **
sod-3 (4) 1 vs 4: **
G
WT (1)
sod-4 (2) 1 vs 2: ns
sod-5 (3) 1 vs 3: **
sod-1; 2; 3; 4; 5 (4) 1 vs 4: ****
H
H2S
H2S
Detoxification
ETC
remodeling
ROS
SODs
HIF-1
SKN-1
DAF-16
adaptative responses

Figure 2—figure supplement 1

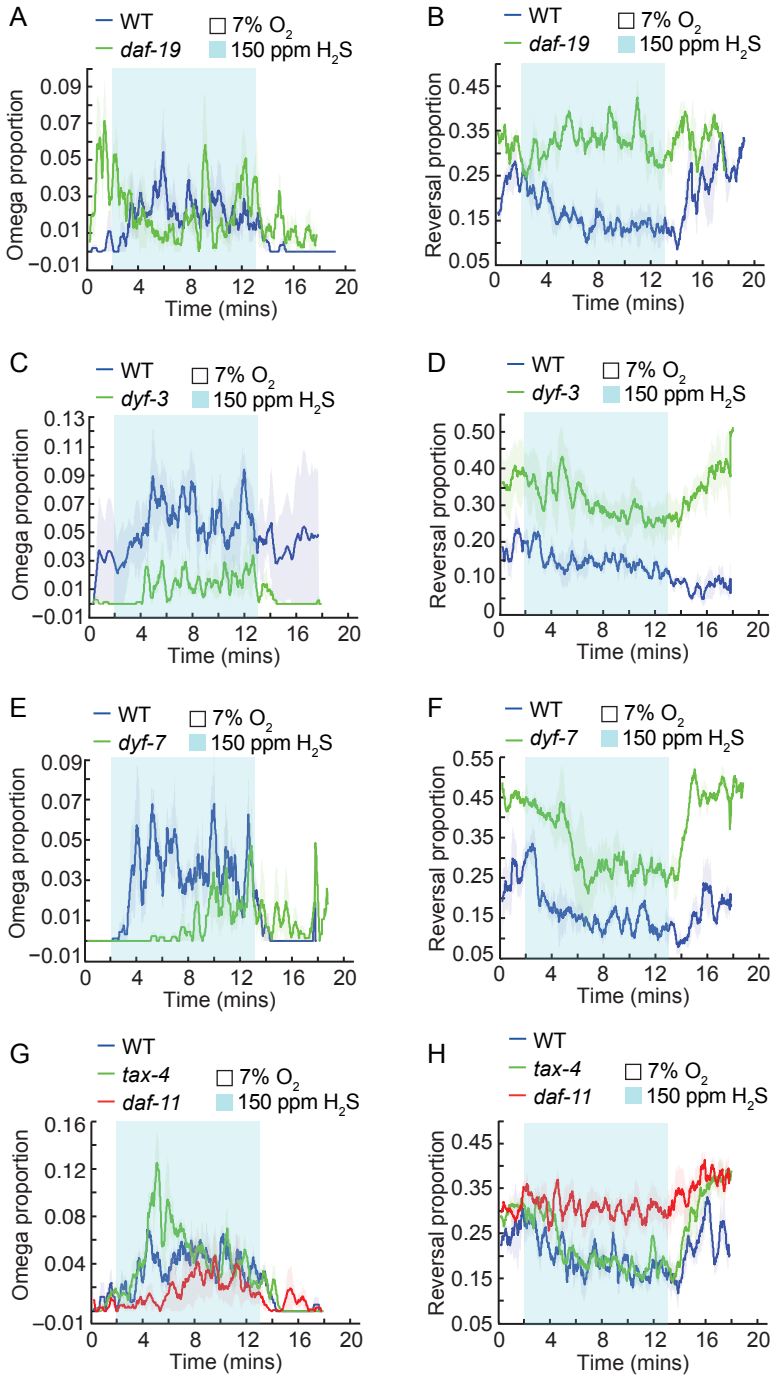

Figure 2—figure supplement 2

A

Promoter	neurons															
Pdaf-11	ASH	AWB	AWC	ASJ	ASK	ADL	ASI	ASE								
Podr-3	ASH	AWB	AWC						ADF	AWA						
Podr-1		AWB	AWC	ASJ	ASK		ASI									
Pflp-21	ASH					ADL	ASI	ASE			FLP	URA	RMG	MC	M2	M4
Pgpa-11	ASH					ADL										
Psra-6	ASH						ASI									PVQ
Ptrx-1				ASJ												

B

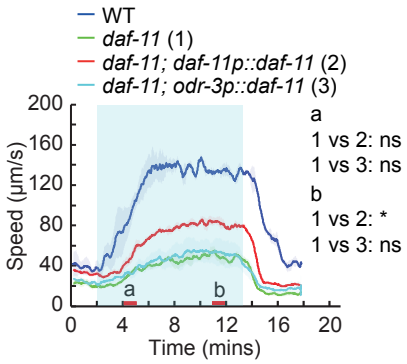

C

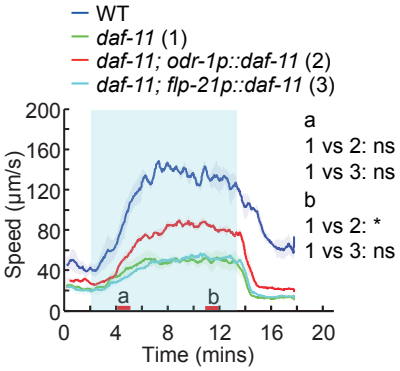

D

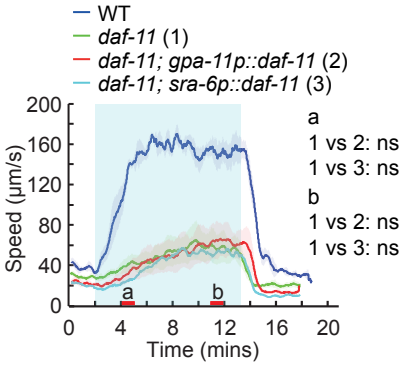

E

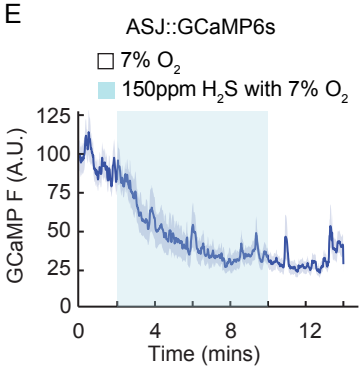

F

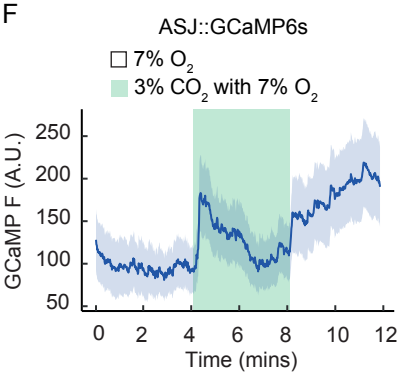

Figure 3—figure supplement 1

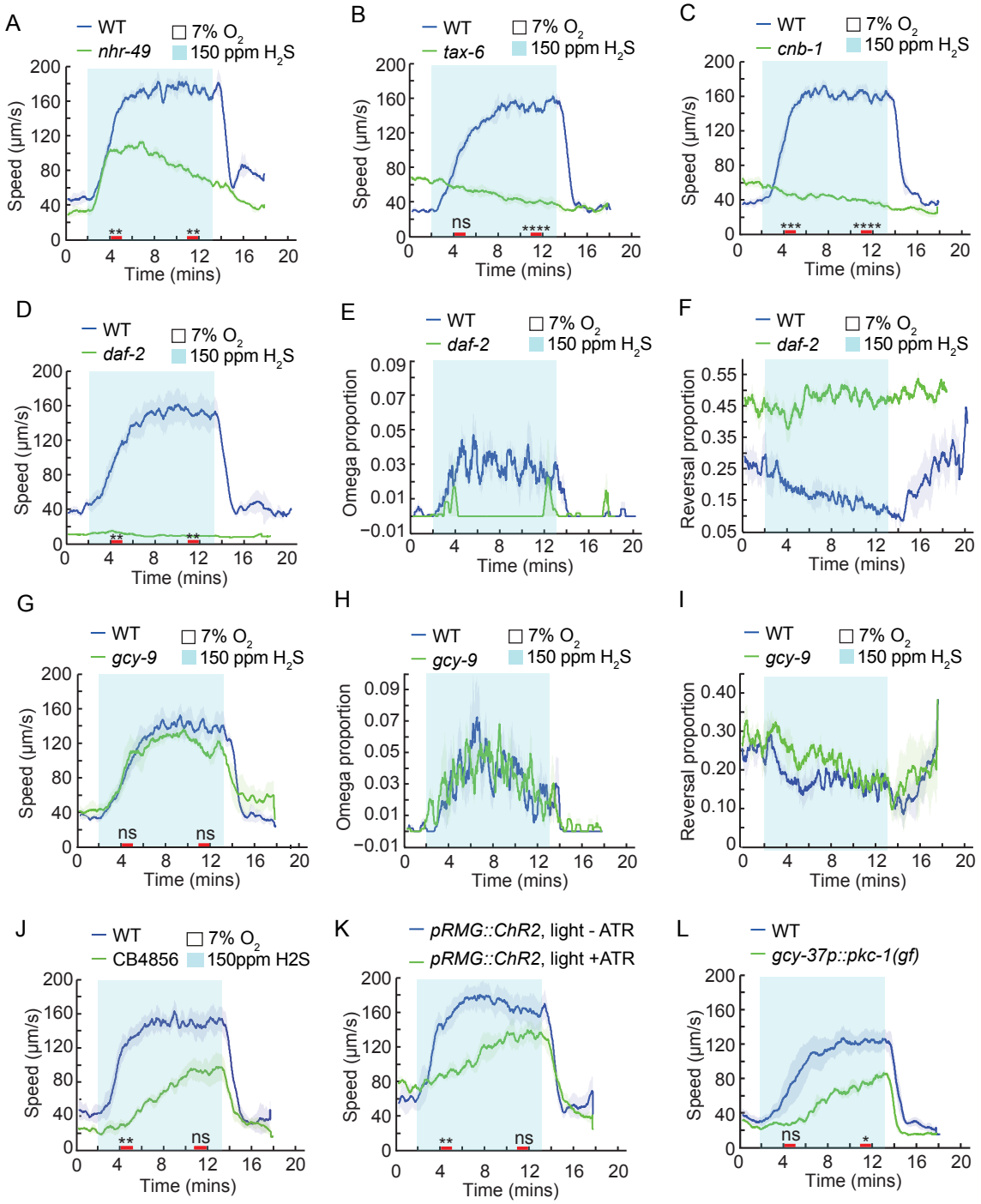

Figure 4—figure supplement 1

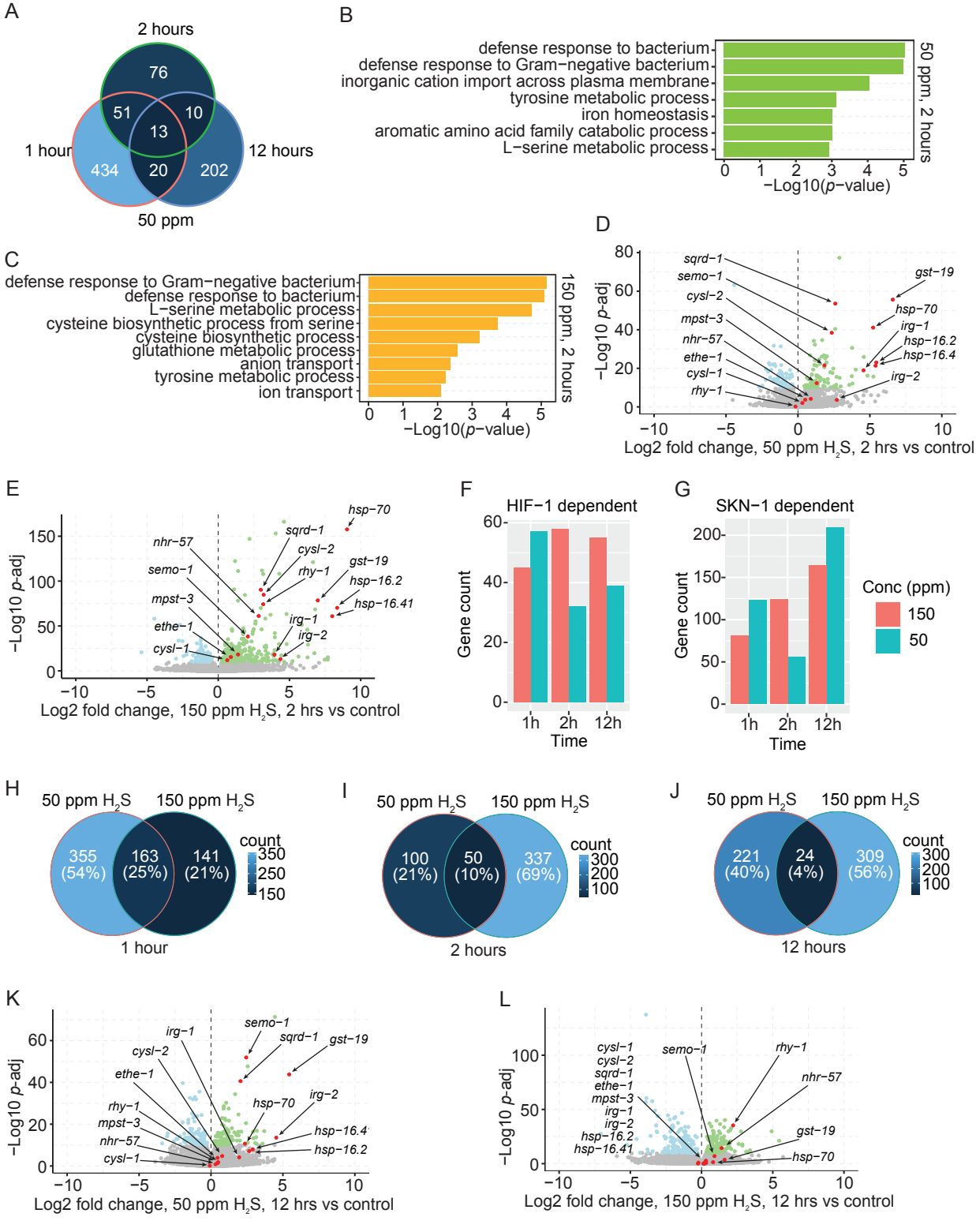

Figure 5—figure supplement 1

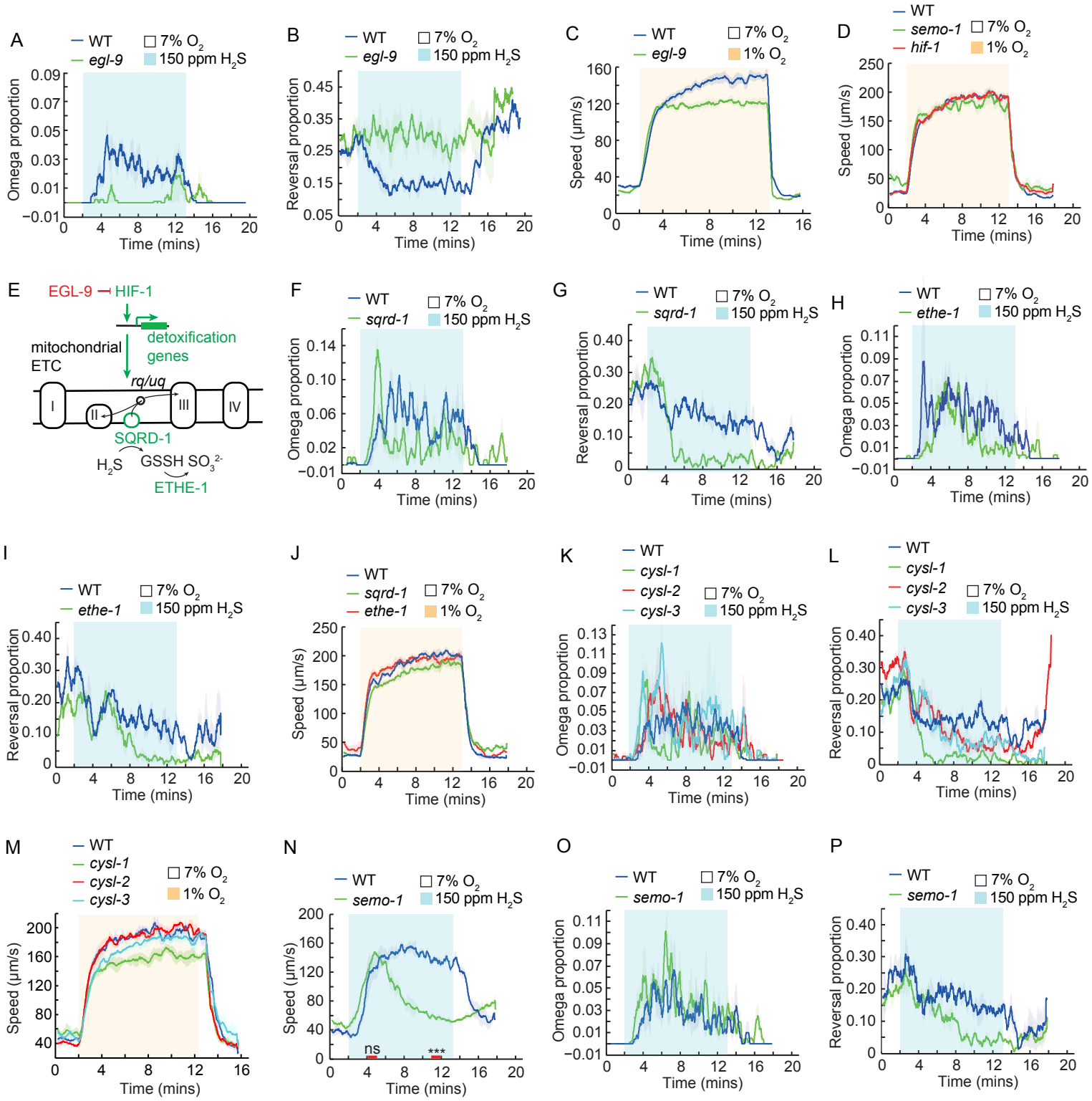

Figure 6—figure supplement 1

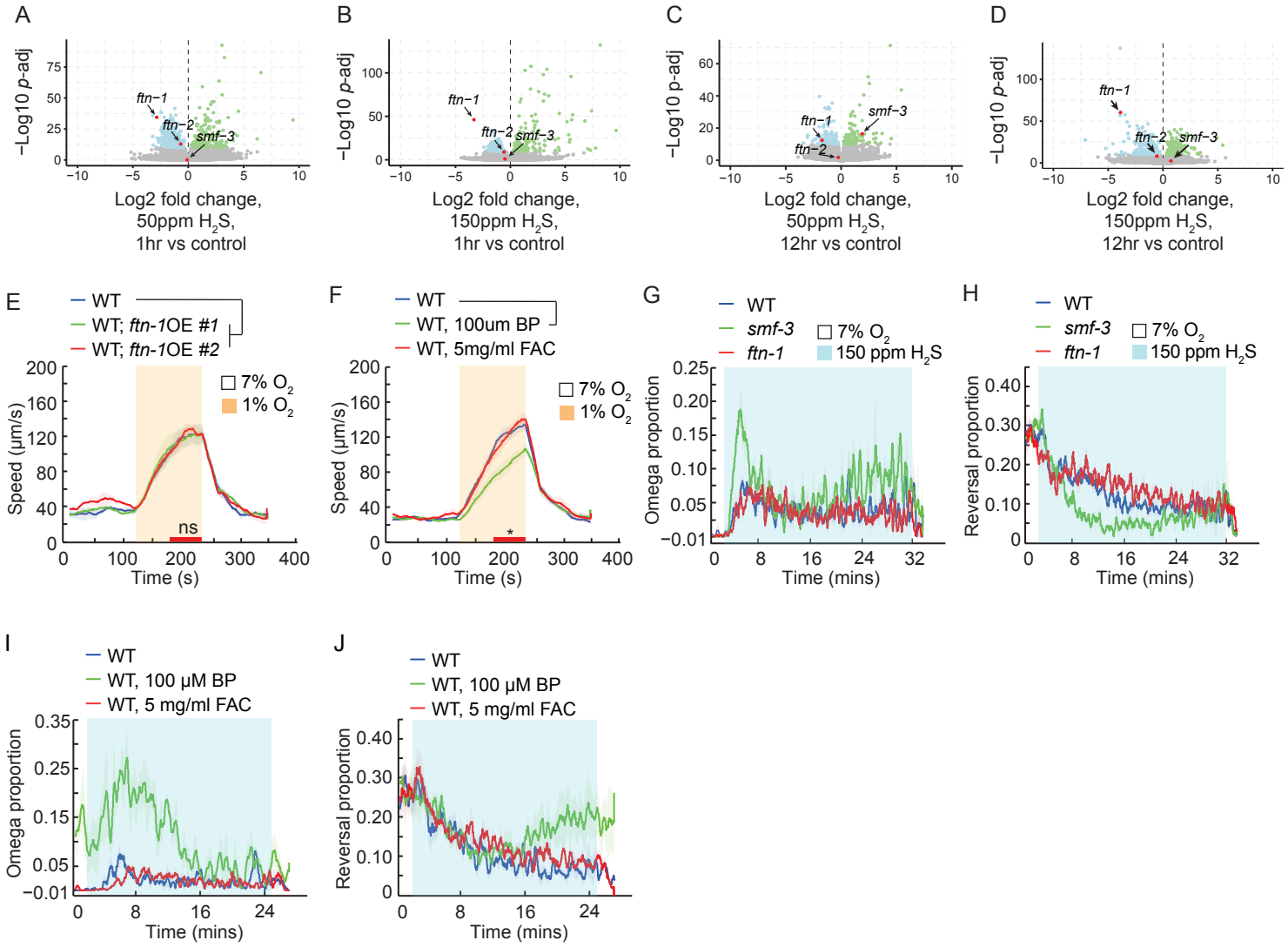
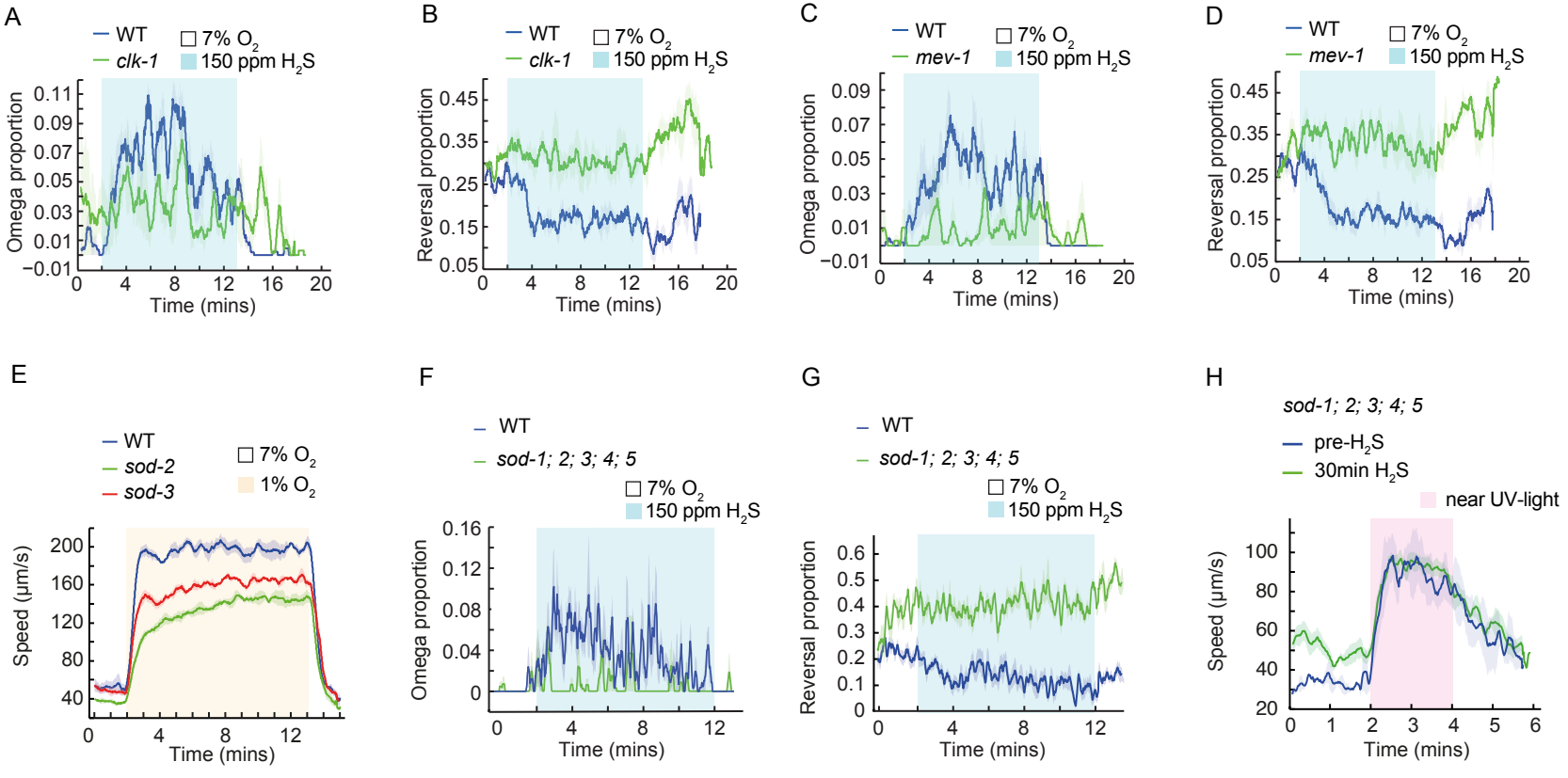
Figure 7—figure supplement 1